AD_____

Award Number: W81XWH-04-1-0644

TITLE: Targeting Breast Cancer CNS Metastasis with Oncolytic Polioviruses

PRINCIPAL INVESTIGATOR: Matthias Gromeier, M.D.

CONTRACTING ORGANIZATION: Duke University
Durham, NC 27708-0491

REPORT DATE: September 2005

TYPE OF REPORT: Final

PREPARED FOR: U.S. Army Medical Research and Materiel Command
Fort Detrick, Maryland 21702-5012

DISTRIBUTION STATEMENT: Approved for Public Release;
Distribution Unlimited

REPORT DOCUMENTATION PAGE

Form Approved
OMB No. 0704-0188

1. REPORT DATE *(DD-MM-YYYY)*	2. REPORT TYPE	3. DATES COVERED *(From - To)*
01-09-2005	Final	6 Aug 2004 – 5 Aug 2005

4. TITLE AND SUBTITLE
Targeting Breast Cancer CNS Metastasis with Oncolytic Polioviruses

5a. CONTRACT NUMBER

5b. GRANT NUMBER
W81XWH-04-1-0644

5c. PROGRAM ELEMENT NUMBER

6. AUTHOR(S)
Matthias Gromeier, M.D.

E-mail: grome001@mc.duke.edu

5d. PROJECT NUMBER

5e. TASK NUMBER

5f. WORK UNIT NUMBER

7. PERFORMING ORGANIZATION NAME(S) AND ADDRESS(ES)
Duke University
Durham, NC 27708-0491

8. PERFORMING ORGANIZATION REPORT NUMBER

9. SPONSORING / MONITORING AGENCY NAME(S) AND ADDRESS(ES)
U.S. Army Medical Research and Materiel Command
Fort Detrick, Maryland 21702-5012

10. SPONSOR/MONITOR'S ACRONYM(S)

11. SPONSOR/MONITOR'S REPORT NUMBER(S)

12. DISTRIBUTION / AVAILABILITY STATEMENT
Approved for Public Release; Distribution Unlimited

13. SUPPLEMENTARY NOTES

14. ABSTRACT
Breast cancer is the most common malignancy in women responsible for >200,000 new cases/yr in the US. Early detection and surgical/radiation therapy can eliminate cancerous growths, but in many cases, late complications result in metastatic spread frequently involving the central nervous system (CNS). There are currently no effective treatments for CNS metastasis of breast cancer and, therefore, this condition is almost invariably fatal. We have developed a new cancer treatment strategy specifically tailored to target and destroy malignant tumors arising in the CNS. Our treatment is based on poliovirus, that we have genetically manipulated to eliminate its diseasecausing properties. Poliovirus naturally targets a cellular protein named CD155, which is normally expressed in CNS motor neurons. However, we discovered that CD155 is abnormally expressed in many cancer cells, including breast cancer. We have made poliovirus clinically applicable by manipulating a crucial genetics regulatory element that is selectively active in cancer cells but cannot function properly in normal CNS neurons. Our research has documented the relationship of CD155 with breast cancer and unraveled the molecular mechanism of cancerspecific function of the human rhinovirus internal ribosomal entry site. The prototype oncolytic poliovirus recombinant PVS-RIPO has been manufactured for clinical use and will be introduced into the clinic in 2006. our pre-clinical studies on breast cancer will help to make this treatment available to breast cancer patients.

15. SUBJECT TERMS
breast cancer, poliovirus, CD155, IRES, oncolytic virus

16. SECURITY CLASSIFICATION OF:			17. LIMITATION OF ABSTRACT	18. NUMBER OF PAGES	19a. NAME OF RESPONSIBLE PERSON
					USAMRMC
a. REPORT	b. ABSTRACT	c. THIS PAGE			19b. TELEPHONE NUMBER *(include area code)*
U	U	U	UU	44	

TABLE OF CONTENTS

INTRODUCTION

We have developed a novel cancer treatment strategy based on genetically engineered polioviruses. Our research conducted under the above referenced award established the relationship of the poliovirus receptor CD155 with breast cancer cells in culture and in patients' tumors. Ectopic expression of CD155 naturally confers target tropism for breast cancer cells to poliovirus. We demonstrated that this relationship can be exploited for therapeutic intervention in a rat xenograft model for breast cancer solitary CNS metastasis. Our research has revealed that there are significant differences with regard to CD155 expression levels amongst individual breast cancer cases, a fact that will necessitate pre-enrollment testing of breast cancer patients for clinical intervention with oncolytic poliovirus recombinants. Most importantly, we have unraveled the molecular mechanism that renders poliovirus replicating under control of a heterologous internal ribosomal entry site (IRES) of human rhinovirus type 2 safe for use in humans. We showed that incompatible protein(host):RNA(virus) interaction at the rhinovirus IRES prevents viral gene expression, particle propagation and cell killing in neuronal cells, the natural target of poliovirus in the human CNS. However, the foreign IRES function is unhindered in malignant cells, e.g. breast cancer cells. Based on our research and the impending introduction of a prototype oncolytic poliovirus recombinant, we propose to extend clinical investigations to patients suffering from CNS complications of breast cancer metastasis.

KEY RESEARCH ACCOMPLISHMENTS

SPECIFIC AIM I.

- Association of CD155 with breast cancer cell lines and patients' tumors
- Relative CD155 levels correlate with susceptibility to PVS-RIPO
- High therapeutic potential for PVS-RIPO in rat xenograft models
- Pre-trial testing of patient breast cancer samples in preparation for clinical trials

SPECIFIC AIM II.

- Elucidation of the molecular mechanism of tumor-specific propagation of PVS-RIPO
- Fundamentally different conditions for translation initiation at the IRES in cancer vs. neuronal cells
- Tumor selective IRES function is mediated by specific binding of NFAR-1 proteins in neuronal cells

REPORTABLE OUTCOMES

SPECIFIC AIM I. *Analyze the association of CD155 with breast cancer.* We have developed a combined antigen capture/immunoblot assay to reliably detect the poliovirus receptor CD155 in breast cancer cell lysates and patients' tissues (Fig. 1A, B) (Ochiai *et al.*, 2004; Appendix I). Our results indicate that CD155 is expressed at very high levels in a proportion of laboratory-established breast cancer cell lines (mediating exquisite susceptibility to the oncolytic PVS-RIPO; Fig. 1C), but present at levels too low to permit complete destruction of monolayer cultures in approximately half of the lines tested (Fig. 1A, C). Interestingly, we observed a similar distribution of CD155 expression levels in breast cancer tissues (Fig. 1B) (Ochiai *et al.*, 2004). CD155 levels appeared to correlate with susceptibility to the prototype oncolytic PVS-RIPO (Fig. 1C).

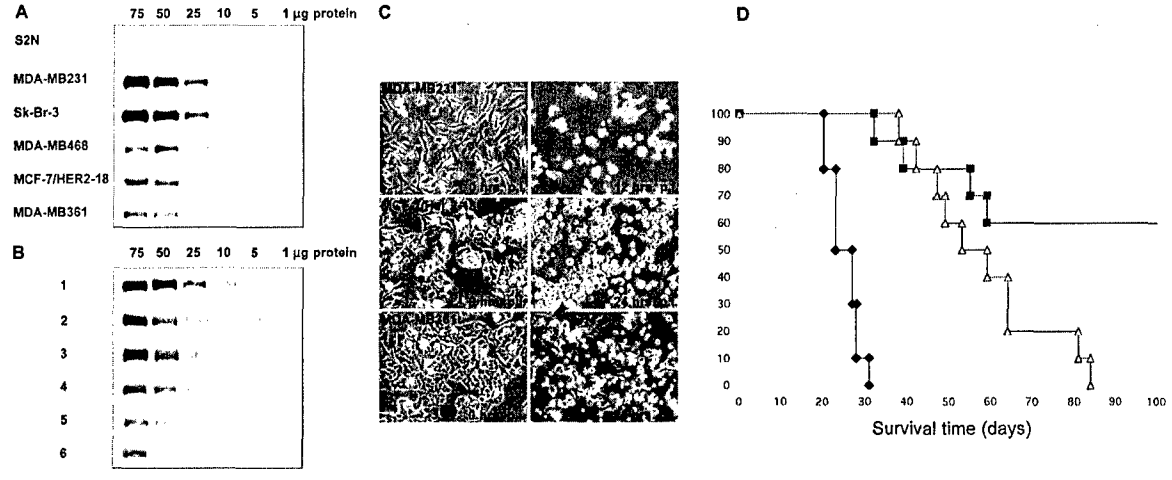

Fig. 1. CD155 expression in breast cancer cells/S2N normal breast epithelium (A) and patient tumors (B). C. CD155 levels correlate with PV susceptibility: MDA-MB231 are lysed 12 hrs post infection (p.i.), but MDA-MB361 partially resist even 24 hrs p.i. D. PVS-RIPO ($\Delta=10^7$;$\blacksquare=10^9$ pfu) has strong anti-neoplastic activity in rat intrathecal breast cancer (MCF-7) xenografts.

Treatment of breast cancer solitary cerebral xenografts in rats with PVS-RIPO resulted in efficient tumor killing (Fig. 1D). This was despite the fact that we had to use MCF-7 (only this cell line is suitable for CNS xenografting) in our studies; MCF-7 is a cell lines with moderate to low CD155 levels (Fig. 1A). Partial resistance of MCF-7 monolayers to infection with MCF-7

(Fig. 1C) is likely related to insufficient CD155 expression. We speculate that incomplete clinical responses in xenografted rats receiving PVS-RIPO is due to low CD155 expression. We have obtained MDA-MB231 cells from Dr. J. Price (M.D. Anderson Cancer Center, Houston, Tx) that were adapted to intracerebral growth by serial passagine via intracarotid inoculation in mice. We will separately assess the oncolytic activity of PVS-RIPO against these cells, which express very high levels of CD155. In a clinical setting only tumors #1-3 (Fig. 1B), expressing CD155 at levels comparable to MDA-MB231 would be eligible for enrollment into clinical studies.

High CD155 levels in at least 50% of the small sample studies (we analyzed tumor tissues from 6 patients) bode well for clinical use of PVS-RIPO in a subset of breast cancer patients. However, the fact that high CD155 expression was not universal amongst breast cancer cases demands that any clinical investigation would have to include pre-enrollment testing for CD155 expression in tumor tissues (these tests have been standardized and are established specifically for this purpose). Future studies will address whether CD155 expression levels correlate with specific biological properties of breast cancers, e.g. histological/clinical grade, invasiveness. The association of breast cancer with CD155 qualifies these cancers for clinical intervention with oncolytic poliovirus recombinants. Depending on the outcome of phase-I clinical trials in glioblastoma patients, we are preparing PVS-RIPO for further clinical investigation in patients with breast cancer metastasis to the CNS.

SPECIFIC AIM II. *Decipher the molecular mechanism of tumor-specific translation initiation at the IRES element.* The question why PVS-RIPO efficiently grows within and kills cancer cells without damaging its natural target motor neurons is crucial with regard to the planned clinical applications for this agent. We have unraveled the mechanism of tumor-selective function of the HRV2 IRES. First, we demonstrated that this phenotype is due to neuron-specific repression of HRV2 IRES function (Fig. 2). This was established through heterokaryon analyses, fusing HEK293 neuronal to cancer cells (Fig. 2).

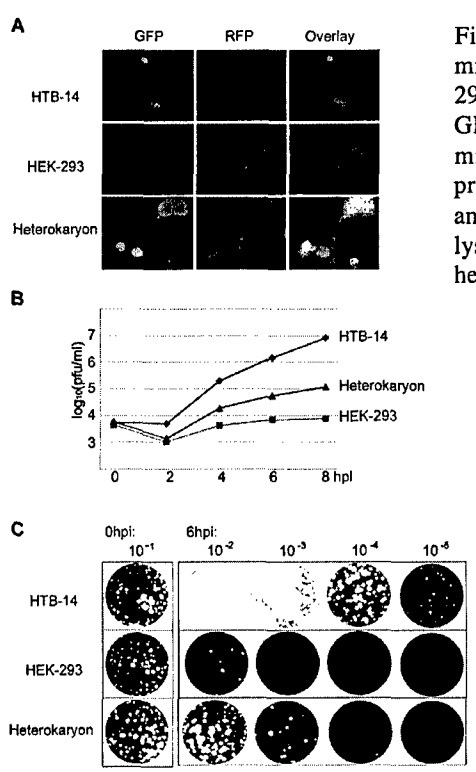

Fig. 2. HEK-293/HTB-14 heterokaryon analysis. A. Fluorescence microscopy of fused HTB-14 cells, fused HEK-293 cells and HEK-293/HTB-14 heterokaryons 2 hrs post fusion. HTB-14 cells express GFP in the cytoplasm and HEK-293 cells express RFP targeted to mitochondria. B. One-step growth curve analysis of PV-RIPO propagation in fused HTB-14 cells (♦), fused HEK-293 cells (■), and HEK-293/HTB-14 heterokaryons (▲). C. Plaque assay of cell lysate diluents from fused HTB-14, HEK-293, and HEK-293/HTB-14 heterokaryons at 0 hrs post infection (hpi) and 6 hpi with PV-RIPO.

Neuron:cancer cells heterokaryons did not support PVS-RIPO propagation, suggesting the cancer-specific growth phenotype to be due to neuron-specific repressors of IRES function (Fig. 2). This is likely to be due to the presence of RNA-binding proteins binding to and inhibiting HRV2 IRES function in neuronal cells (Merrill *et al.*, 2005; Appendix II).

Next, we endeavored to identify proteins with HRV2 IRES affinity in neuronal cell extracts. This search revealed proteins of the NFAR-1 complex to bind to the HRV2 IRES (Merrill *et al.* 2005). We observed that HRV2 IRES binding specifically

occurred with neuronal extracts, but not with cell extracts prepared from cancerous cells (Fig. 3). This suggested that cancer-specific IRES binding activity of NFAR-1 proteins is responsible for tumor-specific cytotoxicity of PVS-RIPO. Analysis of the ribosomal profile of neuronal (HEK293) and cancerous cells revealed a potential mechanism for translation inhibition at the HRV2 IRES by NFAR-1 proteins: cytoplasmic extracts of mock or PVS-RIPO-infected cells were subjected to density gradient centrifugation/fractionation (Fig. 4). Protein composition was assayed in every other fraction while ribosomal and viral RNA (in infected cells) were analyzed in each sample. In uninfected HEK-293 cells, DRBP76 and NF45 co-sediment with free protein, 40S and 60S subunits, mono- and polysomes, while RHA associates exclusively with mono- and polysomes (Fig. 4A). We excluded non-specific co-sedimentation of NFAR-1 proteins in macromolecular complexes with polysomal fractions by treating samples with EDTA (Fig. 4C). Ribosomal protein S6 (RpS6) marks the presence of ribosomes and tubulin represents free protein. In PVS-RIPO infected HEK-293 cells (Fig. 4B) viral RNA is detected mainly in 40S subunit-containing fractions. Retention of PV-RIPO RNA with 40S subunits indicates hindrance of translation initiation at the HRV2 IRES prior to 60S subunit joining.

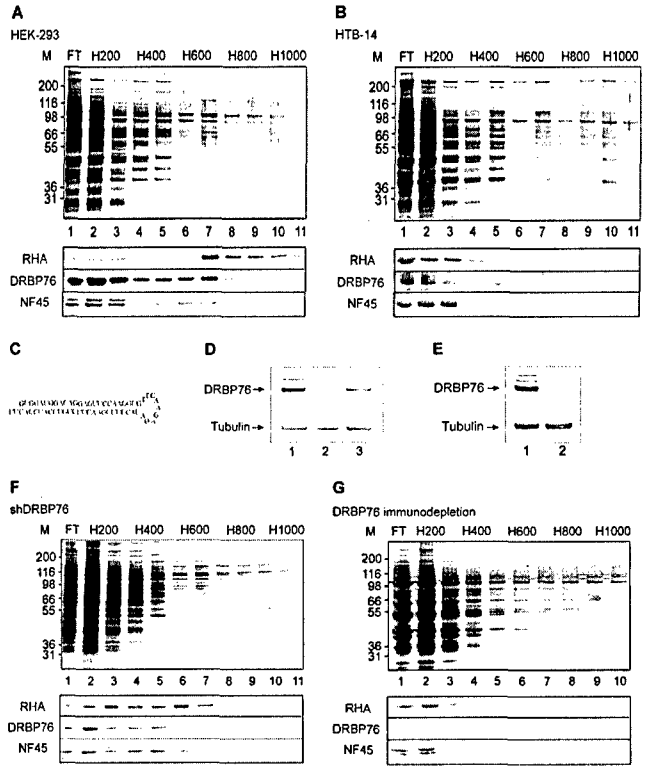

Fig. 3. Comparative RNA affinity chromatography. HEK-293 (A), HTB-14 (B), shDRBP76 (F) and DRBP76 immunodepleted HEK-293 (G) S10 cytoplasmic lysates were applied to sldV/VI RNA affinity columns. After collection of FT (lane 1), the column was washed with H200 (lanes 2-3) and eluted with a 400-1000 mM KCl gradient (lanes 4-11). Column fractions were analyzed by SDS-PAGE and silver stain or Western blot with α-RHA, α-DRBP76 and α-NF45 antibodies as indicated. (C) Sequence and predicted structure of the DRBP76 shRNA. (D) Western blot analysis of control cells (lane 1), shDRBP76 cells (lane 2), and shDRBP76 cells transfected with DRBP76^{mut} DNA (lane 3) using α-DRBP76 and α-tubulin antibodies as indicated. (E) Western blot analysis of HEK-293 S10 (lane 1) and DRBP76 immunodepleted HEK-293 S10 lysate (lane 2) using α-DRBP76 and α-tubulin antibodies as shown.

PV-RIPO infection of HEK-293 cells dramatically shifts the sedimentation pattern of NFAR-1 proteins: polysomal association was lost by 4 hpi, at which point they are detected almost entirely in fractions containing free protein or both 40S subunits and PV-RIPO RNA (Fig. 4B). This effect is not due to a shift of ribosomes from the polysome to the monosome pool because the relative absorbance pattern did not change significantly upon infection.

Wild-type poliovirus is not encumbered to replicate in neuronal cells. Therefore, we also analyzed viral RNA and the NFAR-1 complex in ribosomal profiles from wild-type polio-infected HEK-293 cells. Poliovirus RNA was enriched in polysomal fractions (Fig. 4D). As with PV-RIPO-infected HEK-293 cells, NFAR-1 proteins were released to pre-polysomal fractions; however, in contrast to PV-RIPO, their distribution in the gradient did not overlap with viral RNA (Fig. 4D).

NFAR-1 protein abundance was significantly less in ribosome-containing fractions of cancer relative to HEK-293 cells (Fig. 4A, E). NF45 and RHA are detected in pre-monosomal and monosomal fractions, while DRBP76 does not associate with ribosomes at all. All NFAR-1 proteins from cancer cell lysates co-sediment with free protein. Our data suggest that NFAR-1 proteins associate with the translation apparatus in HEK-293 cells to a greater extent than in cancer cells.

In accordance with efficient viral gene expression in cancer cells, the bulk of PV-RIPO RNA associates with polysomes (Fig. 4F). Unlike HEK-293 cells, virus infection barely affects NFAR-1 distribution in the ribosomal profile. Significantly, there is complete separation of NFAR-1 proteins in pre-monosomal and monosomal fractions from translating viral RNA in polysomes.

We observed neuron-specific binding of NFAR-1 proteins to the HRV2 IRES (Fig. 3) and neuron-specific association with the translation apparatus (Fig. 4A). To investigate if ribosomal association of viral RNA in neuronal cells correlates with the distribution of NFAR-1 proteins, we conducted ribosomal profile analyses in DRBP76 depleted HEK-293 cells (Fig. 3G, H). DRBP76 depletion interrupts HRV2 IRES binding of all NFAR-1 components (Fig. 3F, G) and, thus, may reveal the influence of NFAR-1 proteins on the distribution of viral RNA in the ribosomal profile.

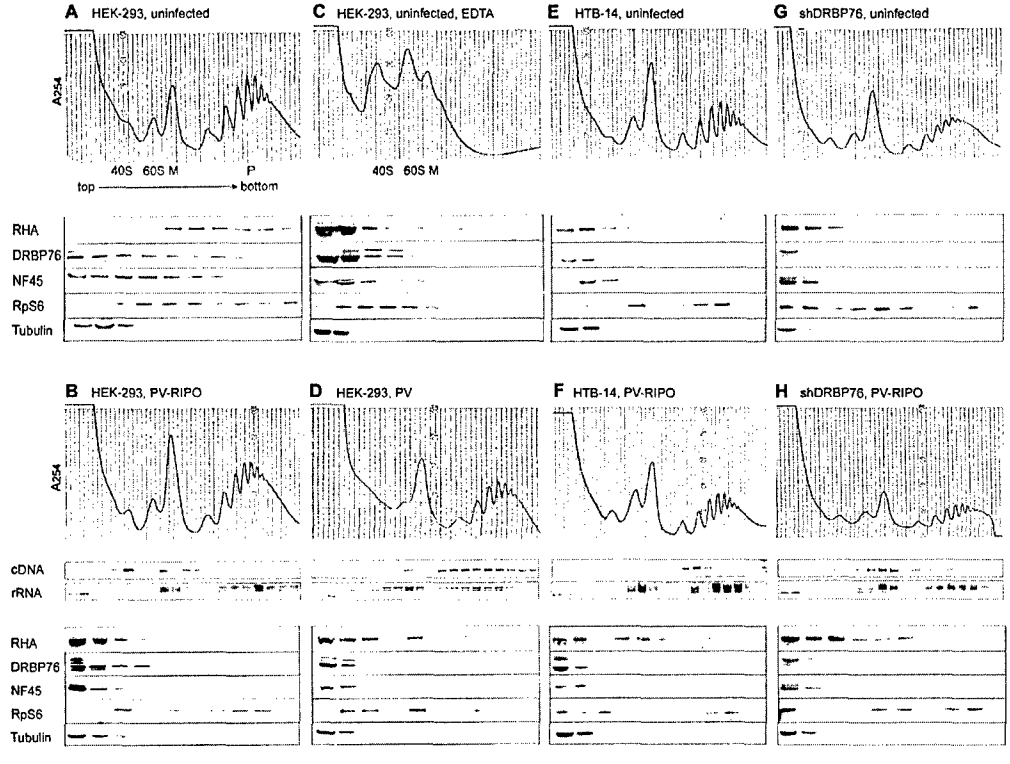

Fig. 4. Ribosomal sedimentation profiles in HEK-293, HTB-14 and shDRBP76 cells. Top panels; A254 absorption spectra of lysates generated from mock infected HEK-293 (A), HTB-14 (E) and shDRBP76 cells (G), or HEK-293 lysates treated with EDTA (C). Bottom panels; A254 absorption spectra of lysates generated from PV-RIPO infected HEK-293 (B), HTB-14 (F), shDRBP76 (H) or poliovirus-infected HEK-293 (D) cells. Lysates from infected cells were generated 4 hpi. Western blot analyses of protein from every other gradient fraction were performed with α-RHA, α-DRBP76, α-NF45, α-RpS6 and α-tubulin antibodies, as indicated. Viral cDNA corresponding to the IRES region was amplified by RT-PCR and rRNA was analyzed from total RNA purified from every fraction in the gradient.

DRBP76 knock-down drastically reduced ribosomal associated DRBP76 and displaced RHA and NF45 from polysomal fractions (Fig. 4G). This suggests that polysome association of these proteins in HEK-293 cells hinges at least in part on DRBP76. As a result, NFAR-1 sedimentation patterns in shDRBP76 cells resembled those in cancer cells (Fig. 4E, G). DRBP76 depletion in infected HEK-293 cells conversely affected the distribution of PV-RIPO RNA in the ribosomal profile. Displacement of NFAR-1 proteins from polysomal fractions by DRBP76 depletion produced a shift of viral RNA towards mono- and polysomal fractions (Fig. 4H). Although the degree of polysome association did not reach that in infected HTB-14 cells, the block of translation processing in HEK-293 cells was relieved (Fig. 4B, H). This indicates that inclusion of HRV2 IRES-containing viral genomes in polysomes is induced upon DRBP76 depletion and resulting dissociation of NFAR-1 proteins from polysomes.

Our analyses of the NFAR-1 proteins' dynamic association with the translation machinery suggest a role in repression of PV-RIPO propagation in HEK-293 cells. shDRBP76 and control cells, which had been infected with the backbone lentiviral vector and selected for blasticidin resistance, were subjected to synchronized infection with PV-RIPO to establish the kinetics of viral propagation and HRV2-IRES-driven gene expression (Fig. 5). DRBP76 depletion substantially elevated viral growth; the maximum progeny yield at 7 hpi in shDRBP76 cells exceeded the controls by approximately 20-fold (Fig. 5A). Furthermore, there was a marked increase in viral gene expression (Fig. 5B). In contrast, DRBP76 depletion had no effect on virus replication or gene expression of wild-type poliovirus (Fig. 5C, D). To exclude non-specific or off-target effects of shRNA-mediated knock-down, we reconstituted the protein in shDRBP76 cells by transfecting a DRBP76 cDNA modified by silent mutagenesis in the region targeted by the shRNA. DRBP76 complementation yielded wild-type levels of the protein (Fig. 3D) and completely reversed the viral growth-enhancing effect of the knock-down (Fig. 5A). Similarly, PV-RIPO gene expression was severely depressed upon reconstitution of DRBP76 (Fig. 5B).

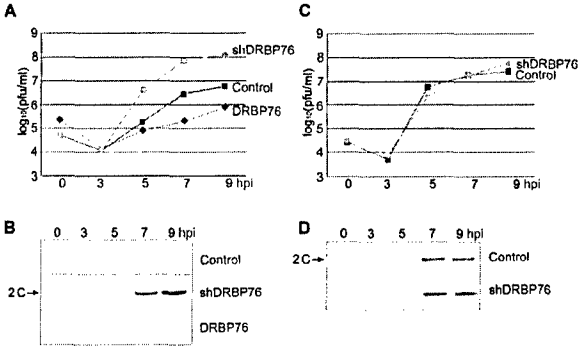

Fig. 5. DRBP76 depletion enhances HRV2 IRES-driven reporter translation, PV-RIPO gene expression and virus propagation in HEK-293 cells. One step growth curve analysis of PV-RIPO (**A**) and PV (**C**) propagation in control cells (■), shDRBP76 cells (●) or shDRBP76 cells transfected with pDRBP76^{mut} DNA (♦). Western blot analysis of PV-RIPO (**B**) and PV (**D**) gene expression in infected cell lysates at specified hpi using α-2C antibody.

Our results demonstrate how neuron-specific binding of DRBP76 (and, possibly, of the intact NFAR-1 complex) selectively abrogates viral replication in neuronal cells without affecting viral propagation and cytotoxicity in cancer cells (Merrill *et al.*, 2005). Currently, we are investigating the precise mechanism of translation arrest at the HRV2 IRES by NFAR-1 complex through toe-printing and high-resolution ribosomal profile analysis as well as the involvement of individual NFAR-1 proteins vs. the entire complex through gel filtration assays. Furthermore, we have begun to investigate expression patterns of NFAR-1 components in tumor tissues from patients.

Elucidation of the molecular basis for tumor specific viral propagation and cell killing of PVS-RIPO are an integral part of our efforts to introduce PVS-RIPO and the concept of tumor targeting at the translational level into the clinic.

OTHER PROGRESS. *Introduction of PVS-RIPO into the clinic.* The prototype oncolytic polio/rhinovirus chimera PVS-RIPO has been gmp-manufactured at the NCI, has passed recombinant DNA advisory committee (RAC) review in June '05 and is currently undergoing toxicology evaluations in *CD155* transgenic mice and non-human primates at the NCI. A pre-IND meeting is scheduled with the FDA and we anticipate phase-I clinical trials against glioblastoma multiforme to begin at the Duke University Medical Center in late 2006. With positive results from these initial clinical studies, we would extend clinical investigations to CNS neoplasms secondary to systemic cancer, e.g. breast cancer.

CONCLUSIONS

We have established a new cancer treatment regimen targeting abnormal expression of the poliovirus receptor CD155 in breast cancer. We have established the molecular parameters mediating specific target tropism and selective viral replication in cancerous cells. Introduction of our approach into the clinic is imminent.

REFERENCES

Merrill M, Dobrikova E, Gromeier M (2005) Cell-type specific repression of internal ribosome entry site activity by the NFAR-1 complex; *EMBO J*, submitted; (Appendix II).

Ochiai H, Moore S, Archer GE, Okamura T, Chewning TA, Marks JR, Sampson JH, Gromeier M (2004) Treatment of intracerebral neoplasia and neoplastic meningitis with regional delivery of oncolytic recombinant poliovirus. *Clin Cancer Res* 10:4831-8; (Appendix I).

APPENDIX I

Vol. 10, 4831–4838, July 15, 2004

Treatment of Intracerebral Neoplasia and Neoplastic Meningitis with Regional Delivery of Oncolytic Recombinant Poliovirus

Hidenobu Ochiai,[1] Stephanie A. Moore,[3] Gary E. Archer,[1] Tatsunori Okamura,[1] Tracy A. Chewning,[1] Jeffrey R. Marks,[2] John H. Sampson,[1] and Matthias Gromeier[3]

[1]Division of Neurosurgery, Department of Surgery; [2]Department of Surgery; and [3]Department of Molecular Genetics and Microbiology; Duke University Medical Center, Durham, North Carolina

ABSTRACT

Purpose: **Spread to the central nervous system (CNS) and the leptomeninges is a frequent complication of systemic cancers that is associated with serious morbidity and high mortality. We have evaluated a novel therapeutic approach against CNS complications of breast cancer based on the human neuropathogen poliovirus (PV).**

Experimental Design: **Susceptibility to PV infection and ensuing rapid cell lysis is mediated by the cellular receptor of PV, CD155. We evaluated CD155 expression in several human breast tumor tissue specimens and cultured breast cancer cell lines. In addition, we tested an oncolytic PV recombinant for efficacy in xenotransplantation models of neoplastic meningitis and cerebral metastasis secondary to breast cancer.**

Results: **We observed that breast cancer tissues and cell lines derived thereof express CD155 at levels mediating exquisite sensitivity toward PV-induced oncolysis in the latter. An association with the immunoglobulin superfamily molecule CD155 renders breast cancer a likely target for oncolytic PV recombinants. This assumption was confirmed in xenotransplantation models for neoplastic meningitis or solitary cerebral metastasis, where local virus treatment dramatically improved survival.**

Conclusions: **Our findings suggest oncolytic PV recombinants as a viable treatment option for CNS complications of breast cancer.**

Received 12/8/03; revised 4/8/04; accepted 4/13/04.

Grant support: USPHS Grant CA87537 (to M. Gromeier). M. Gromeier is a recipient of a Burroughs Wellcome Career Award in the Biomedical Sciences.

The costs of publication of this article were defrayed in part by the payment of page charges. This article must therefore be hereby marked *advertisement* in accordance with 18 U.S.C. Section 1734 solely to indicate this fact.

Note: H. Ochiai and S. Moore contributed equally to this work.

Requests for reprints: Matthias Gromeier, Department of Molecular Genetics and Microbiology, Duke University Medical Center, Box 3020, Durham, NC 27710. Phone: (919) 668-6205; Fax: (919) 684-8735; E-mail: grome001@mc.duke.edu.

INTRODUCTION

Dissemination of cancer to the brain or leptomeningeal invasion of metastatic or primary central nervous system (CNS) neoplasms is usually a terminal event for cancer patients (1), resulting in a median survival of generally <1 year (2–9). This dismal prognosis reflects the limitations placed on radiotherapy by (*a*) the significant risk of brain damage and spinal cord radionecrosis, (*b*) the inability to deliver therapeutic drug levels to the brain and cerebrospinal fluid with systemic administration, and (*c*) the minimal efficacy of currently available chemotherapeutic agents approved for intracerebral or intrathecal use (2–9). As a result, new, potent, and selective treatments for metastatic brain tumors and neoplastic meningitis (NM) are desperately needed.

Recently, genetically engineered human pathogenic viruses have emerged as a novel class of putative antineoplastic agents with properties useful in the design of treatment strategies targeting primary or metastatic CNS neoplasms (10–12). Whereas a variety of viral agents are under consideration for use in such strategies, oncolytic agents based on the neuropathogen poliovirus [PV (13)] may have intrinsic properties that render them particularly suitable for targeting neoplastic lesions arising in the CNS.

The antineoplastic activity of viral oncolytic agents depends on efficient targeting and entry into cancer cells expressing appropriate receptor proteins on their surface. Susceptibility to PV is mediated by the cellular receptor of PV, the immunoglobulin superfamily molecule CD155 (14). Only *CD155* gene products in humans (14) and their simian homologs (15) can serve as PV receptors; CD155 alone is sufficient to confer susceptibility to the virus because mice transgenic for the human *CD155* gene develop classic poliomyelitis after PV infection (16, 17).

Most importantly, the human pathogen PV needs to be genetically modified for clinical applications to achieve selective virus replication and cytotoxicity in tumor cells without collateral damage to normal CNS or extraneural tissues. Conditional replication in cancerous cells was achieved by genetic recombination with human rhinovirus type 2 (HRV2). PVs and human rhinoviruses, like all *Picornaviridae*, depend on the internal ribosomal entry site (IRES) within their 5′-nontranslated region for translation initiation of their uncapped (+)-strand RNA genome (18, 19). We have demonstrated that exchange of its cognate IRES with that of HRV2, yielding the chimera PV1(RIPO) (20) and its derivative, PVS-RIPO, drastically reduces PV propagation in cells of neuronal derivation (20). These neural replication deficits ablate the ability of the virus to cause poliomyelitis in CD155 transgenic mice (20, 21) and in intraspinally inoculated cynomolgus macaques (21).

Remarkably, the HRV2 IRES-mediated ablation of neuropathogenic properties does not affect cytopathogenicity for malignant cell types. Selective activity of the HRV2 IRES in

rapidly growing malignant cells suggests fundamental differences in the control of translation rate in cancerous cells, which uniquely exposes these cells to destruction by PVS-RIPO. The molecular mechanisms regulating IRES activity and its cell type-specific restrictions are poorly understood, due to the complexity of potential regulatory influences including canonical translation factors, noncanonical IRES-binding proteins, IRES structure, and interactions with distant regulatory elements within the viral genome (22). We have recently reported that tumor-specific activity of the HRV2 IRES relies on interaction with structural elements of the viral 3′-nontranslated region (23).

In this study, we report the successful use of the prototype oncolytic PV recombinant PVS-RIPO in athymic rat models of breast cancer cerebral metastasis and NM. Intrathecal or intracerebral administration of PVS-RIPO was found highly effective against human breast cancer xenografts growing in the subarachnoid space or brain parenchyma of athymic rats. Our observations suggest that the oncolytic effects of PVS-RIPO are mediated by ectopic expression of the PV receptor CD155 on breast cancer cells. Our approach conceptually resembles successful strategies targeting cell surface molecules of breast cancer cells with monoclonal antibodies (reviewed in Ref. 24). In addition to efficient targeting and destruction of CD155-expressing cancer cells, PVS-RIPO amplification with the possibility of multiple rounds of replication in tumors provides a strong incentive to further investigate the benefits of this novel approach to cancer treatment.

MATERIALS AND METHODS

Human Cell Lines and Virus. Breast cancer cell lines (MDA-MB-361, MDA-MB-468, MDA-MB-231, and Sk-Br-3), glioma cell line U87, and HEK 293 cells were obtained from American Type Culture Collection (Manassas, VA) and propagated according to standard practices. Xenotransplantations were carried out with breast cancer cell line MCF-7/HER2-18, a HER2 cDNA-transfected MCF-7 subclone propagated as described previously (25).

PVS-RIPO was derived from PV1(RIPO) (20) by substituting the coding region of the type 1 live attenuated Sabin [PV1(S)] vaccine strain. Genomic PV1(S) cDNA [provided by A. Nomoto (University of Tokyo, Tokyo, Japan)] was digested with *AvaI*. The resulting 7.0-kb restriction fragment was ligated with a PCR fragment amplified from PV1(RIPOS) (22) with primers 5′-GGGTCGACTAATACGACTCCTATAGTAAAA-CAGCTCTGGGGTTGT-3′ and 5′-CCATTTCTCGGGCACT-GGAGCG-3′ and pBS vector (NEB, Beverly, Massachusetts) digested with *AvaI* and *SalI*. PVS-RIPO cDNA was processed for re-derivation of virus as described previously (20). UV inactivation of virus (13), synchronized infections (20), and one-step growth kinetics (20) were performed as described previously.

Antigen Capture/Western Blot Analysis and Immunocytochemistry. Breast cancer cell monolayers were homogenized in lysis buffer (PBS and 0.5% NP40). Breast cancer tissues were Dounce homogenized in lysis buffer and centrifuged to remove undissolved debris. The protein concentrations in all lysates were determined using the Bradford method. ELISA plates were treated overnight with monoclonal anti-CD155 antibody D171 (16) suspended in carbonate buffer [0.1 M $NaHCO_3$ and 0.03 M Na_2CO_3 (pH 9.5)] and rinsed afterward to remove unbound antibody. Individual wells were filled with lysate at the indicated protein concentration and incubated for 4 h at room temperature. After thorough rinsing, the captured antigen was released with SDS-PAGE loading buffer (23) at 95°C. The recovered material was analyzed by SDS-PAGE and Western blot. Filters were blocked overnight in TBST-B [10 mM Tris (pH 8.0), 150 mM NaCl, 0.05% Tween 20, and 3% dry milk] and treated first with polyclonal anti-CD155 antibody D480 (diluted 1:1000 in TBST-B) and then with biotinylated antirabbit IgG antibody (diluted 1:500 in TBST-B; Vector Laboratories, Burlingame, CA) followed by streptavidin-horseradish peroxidase complex (Roche, Indianapolis, IN) and developed with chemiluminescent ECL substrate (Amersham, Piscataway, NJ). Immunocytochemical analysis of poliovirus antigens 2C/2BC was performed as described previously (23).

Serial Passaging of PVS-RIPO and Sequencing of the Viral Genome. PVS-RIPO recovered after passaging in MCF-7/HER2-18 cells in culture or obtained from intracerebral xenografts of treated rats was subjected to sequencing by reverse transcription-PCR. Serial passages of PVS-RIPO in MCF-7/HER2-18 cells were carried out as described previously (26). Two rats were sacrificed 14 days after intratumoral virus administration, and the remnant intracerebral xenograft tissue was dissected. The tissue was Dounce homogenized, and the resulting extract was used to infect MCF-7/HER2-18 cell monolayers to amplify virus for further analyses. Viral genomic RNA was recovered from infected MCF-7/HER2-18 cells and subjected to reverse transcription-PCR analysis as described previously (26).

Athymic Rat Model of NM and Metastatic Brain Tumor. Subarachnoid catheters were implanted into female athymic BIGNIMR^{nu} rats (190–260 g) using previously established procedures (25, 27, 28). Briefly, anesthetized rats received a midline sagittal incision from the inion to the laminar arch of C1 to expose the atlanto-occipital membrane and open the underlying cisterna magna dura mater. A PE-10 catheter (Intramedic, Franklin Lakes, NJ) with a 5-0 wire stylet was inserted into the subarachnoid space to the lumbar spinal cord (8.5 cm) and secured with dental epoxy.

Similarly, intracerebral catheters were implanted into the right caudate nucleus using previously established procedures (25). Briefly, a 25-gauge guide cannula (Plastics One, Roanoke, VA) was placed 1 mm anterior, 3 mm right from the bregma and 3 mm deep from the outer table of the skull into the brain of anesthetized rats. The cannula was attached to the skull using cranioplasty cement and secluded with a dummy cannula, and the incision was closed with skin staples. All rats were allowed to recover for at least 7 days, and only animals showing normal weight and neurological function with no evidence of infection were used in the experiments.

MCF-7/HER2-18 cells were harvested with cell scrapers and suspended in PBS to yield a concentration of 10^8 cells/ml for intrathecal or 8×10^7 cells/ml for intracerebral inoculation. Isoflurane-anesthetized rats received 1.25×10^7 MCF-7/HER2-18 cells/100 μl via a Hamilton injector (Hamilton, Reno, NV) intrathecally or 8×10^5 MCF-7/HER2-18 cells/10 μl via a 25-gauge blunt needle 7 mm deep to the outer table of the skull through the guide cannula. Before virus treatment, three ran-

domly selected rats harboring intrathecal or intracerebral xenografts each were sacrificed and examined histologically to confirm tumor presence.

Toxicity and Efficacy Studies. For intrathecal and intracerebral toxicity studies, athymic rats received injection with PVS-RIPO at 10^9 plaque-forming units (pfu)/60 μl or 10^7 pfu/10 μl, respectively. Weight, neurological status, survival, and histology of the neuraxis and internal organs were compared with a PBS-treated control group.

For intrathecal efficacy studies, rats in the treatment groups received injection with PVS-RIPO at 10^7 pfu or 10^9 pfu/40 μl, and rats in the control groups received injection with 10^7 pfu of UV-inactivated PVS-RIPO. For intracerebral efficacy studies, rats in the treatment groups received injection with PVS-RIPO at 10^7 pfu/10 μl or 10^9 pfu/20 μl, and rats in the control groups were injected with 10^7 pfu of UV-inactivated PVS-RIPO. Weight, neurological status, survival, and histopathology of the neuraxis were evaluated in all animals. Neurological evaluation included testing of the stepping and placing reflex and the ability to climb a 60-degree incline ramp. Six representative CNS cross-sections, including forebrain at the level of the lateral ventricles, hindbrain at the level of the occipital lobe, and four equidistant spinal cord/cauda equina sections, were evaluated histologically for hemorrhage, necrosis, edema, demyelination, and arachnoid fibrosis.

Statistical Analysis. Survival estimates and median survival were determined according to Kaplan and Meier (29). Survival data were compared by using the non-parametric log rank test.

RESULTS

Association of CD155 with Breast Cancer Mediates Susceptibility to PVS-RIPO. We used a combined antigen capture/SDS-PAGE-Western blot assay (see "Materials and Methods") to evaluate the expression of the PV receptor CD155 in a panel of five breast cancer cell lines and normal human breast ductal epithelium (Fig. 1*A*) and in six breast cancer tissue specimens derived from primary tumor (Fig. 1*B*). Expression of CD155 could barely be detected in normal human breast epithelium (*S2N*) with the very sensitive assay used (Fig. 1*A*; see "Materials and Methods"). CD155 levels in all breast cancer cell lines significantly exceeded the very scant expression in normal breast explant cultures, but they varied considerably among individual cell lines (Fig. 1*A*). Correspondingly, we observed partial resistance to PVS-RIPO cytolysis in MDA-MB-361, the cell line with the lowest expression of CD155 in the panel (Fig. 2). Infection led to the demise of approximately 70% of these cells by 8–12 h postinfection, but that proportion did not increase, even 24 h postinfection, suggesting resistance to PVS-RIPO infection in subpopulations of this culture (Fig. 2). Similarly, low CD155 expression in MCF-7/HER2-18 may explain partial resistance to PVS-RIPO cytolysis (24 h postinfection, ~10% of cells remained intact; Fig. 2). In contrast, MDA-MB-231 cultures with highly elevated CD155 levels were destroyed completely by PVS-RIPO after 12 h (Fig. 2). The remaining two cell lines were efficiently lysed by PVS-RIPO treatment (data not shown), in accordance with CD155 expression levels in excess of MCF-7/HER2-18.

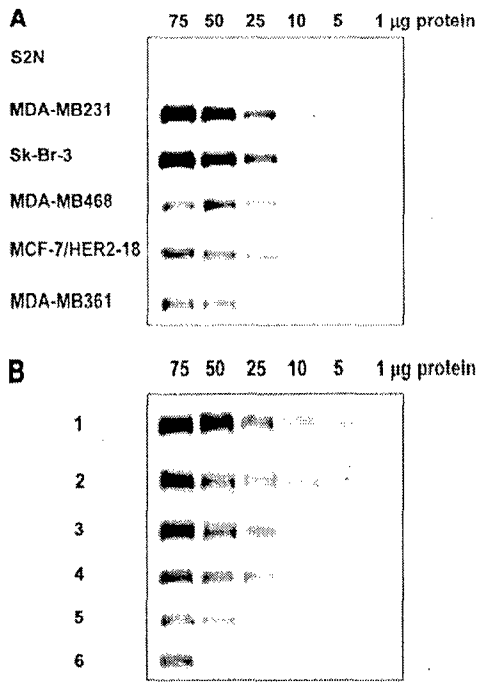

Fig. 1 Expression profiling of the poliovirus receptor CD155 by antigen capture/SDS-PAGE-Western blot (see "Materials and Methods"). CD155 expression was evaluated in primary explant normal ductal epithelium and established breast cancer cell lines (*A*) and in breast cancer tissue specimens (*B*). CD155 was barely detectable in normal breast epithelial cultures (*S2N*), where a trace of signal was apparent with 75 μg of total protein applied. Both the panel of cell lines (*A*) and tumor samples (*B*) displayed a similar range of CD155 expression levels

Variable CD155 expression among established breast cancer cell lines suggests a similar scenario for actual tumor tissues. This assumption was confirmed by analyses of tumor biopsy material, which revealed levels of CD155 expression commensurate with susceptibility to the oncolytic PVS-RIPO in most of the tumors tested (Fig. 1*B*). Interestingly, in the panel of six tumors analyzed, a range of CD155 expression levels similar to that found among breast cancer cell lines was observed (Fig. 1*B*). Although direct comparison with cultured cells may be inaccurate due to the complex composition of tumor tissue, scarce CD155 expression in tumors 5 and 6 at levels corresponding to MDA-MB-361 cells may preclude susceptibility to the oncolytic effects of PVS-RIPO. High levels of CD155 expression corresponding to fully susceptible cell lines in most specimens (Fig. 1*B*) suggest breast cancer cells to be excellent targets for PV-based biotherapeutic agents. The panel of tissue specimens analyzed consisted of primary tumors, and no additional phenotypic or genotypic markers were available. We are currently evaluating a correlation of CD155 expression with additional phenotypic and genotypic markers in a larger set of tumors.

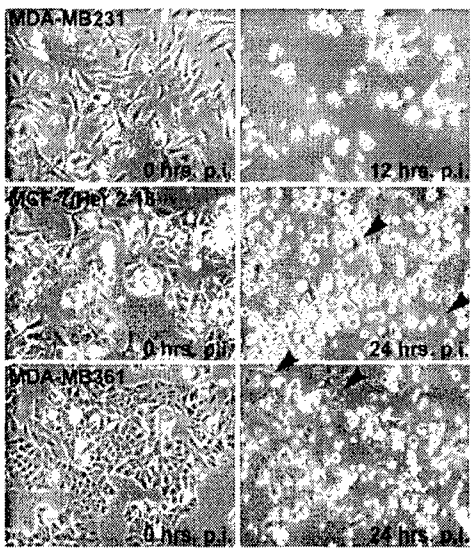

Fig. 2 Susceptibility to PVS-RIPO corresponds to relative expression levels of CD155 (compare with Fig. 1*A*). Cells were infected with PVS-RIPO at a multiplicity of infection of 10 and monitored for 24 h. The *arrowheads* indicate surviving cells that resist infection. MDA-MB-231 cells were completely lysed by 12 h postinfection, whereas a very minor proportion of MCF-7/HER2-18 cells and a substantial subfraction of MDA-MB-361 cells resisted destruction even 24 h postinfection.

The Dynamics of PVS-RIPO-Mediated Killing of MCF-7/HER2-18. To evaluate the oncolytic capacity of PVS-RIPO in breast cancer cells expressing CD155, we chose MCF-7/HER2-18 with CD155 levels exceeding normal breast epithelium ~25-fold but ~2–10-fold lower than MDA-MB-231 and Sk-Br-3 (Fig. 1*A*). The main motivation for our choice was the fact that MCF-7 is the only line known to form established xenografts after intrathecal administration into athymic rodents (25). Analyses of one-step growth kinetics revealed very efficient propagation of PVS-RIPO in MCF-7/HER2-18 cells in step with replication in highly susceptible U87 malignant glioma cells (13) and HeLa R19 cells used for the propagation of PVs in the laboratory (Ref. 20; Fig. 3*A*). Efficient particle propagation corresponded to robust viral gene expression in infected cells (Fig. 3*B*). These findings demonstrate that the cytolytic effect of PVS-RIPO mediated by CD155 coincides with intracellular virus gene expression and particle propagation. Ultimately, the expression of cytotoxic viral gene products and rampant particle propagation lead to lytic destruction of tumor cells (see Fig. 2*B*).

Efficacy of PVS-RIPO against NM in a Human Breast Cancer Xenograft. To test the oncolytic activity of PVS-RIPO against MCF-7/HER2-18-induced NM *in vivo*, we established intrathecal xenografts in athymic rats as outlined in "Materials and Methods." Leptomeningeal tumor was evident microscopically 3 days after intrathecal tumor challenge with 1.25×10^7 MCF-7/HER2-18 cells and resulted in tumor growth in all rats challenged. All untreated rats died from leptomeningeal tumors (Fig. 4). We evaluated the toxicity of our approach in nonxenografted rats treated with PVS-RIPO *versus* PBS as well as efficacy in animals harboring xenografts treated with PVS-RIPO *versus* UV-inactivated virus.

Because rats do not express CD155 and, hence, are resistant to PV infection, the occurrence of virus-induced toxicity in these animals on infection is unlikely. This expectation was confirmed by the dedicated leptomeningeal toxicity study. Groups of six athymic rats without xenografts receiving intrathecal delivery of either PVS-RIPO (10^9 pfu in 60 μl of PBS) or PBS alone experienced neither weight loss of >10% nor neurological deficits. Histological examination of the neuroaxis revealed mild peri-catheter demyelination of spinal cord in four rats in the PBS-treated group and two rats in the PVS-RIPO-treated group. These asymptomatic lesions, which are likely due to catheter placement, are commonly seen in studies using this tumor model (25, 27, 28). No evidence of hemorrhage, necrosis, edema, or arachnoid fibrosis was identified in the brain or spinal cord of PVS-RIPO-treated rats, and histological examination of internal organs including heart, lung, liver, spleen, and kidney of each rat showed no abnormalities.

The therapeutic efficacy of PVS-RIPO against MCF-7/HER2-18-induced NM was investigated in groups of 10 rats treated with two different doses administered intrathecally and

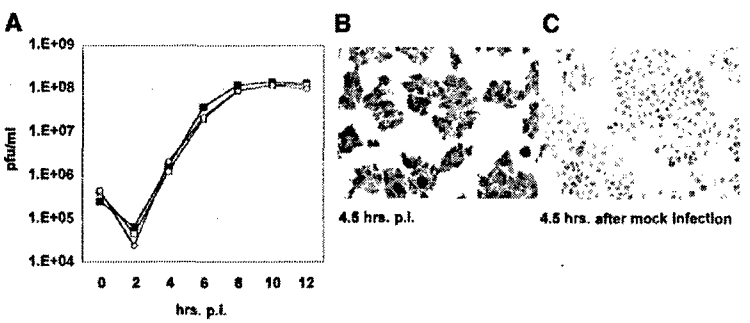

Fig. 3 PVS-RIPO propagation and gene expression in breast cancer cells. *A*, one-step growth kinetics of PVS-RIPO indicate efficient viral replication in MCF-7/HER2-18 (■), HeLa (○), and U87 (□) cells. *B*, PVS-RIPO-infected MCF-7/HER2-18 cells stain strongly for poliovirus 2C/2BC antigens.

compared with a group of 10 rats treated with UV-inactivated PVS-RIPO. Treatment with PVS-RIPO 3 days after inoculation of 1.25×10^7 MCF-7/HER2-18 cells increased median survival by 130% from 23 days in the UV-inactivated virus-treated group to 53 days in the group treated with 1×10^7 pfu of PVS-RIPO ($P < 0.0001$; Fig. 4). In the group receiving a higher dose of 1×10^9 pfu of PVS-RIPO, the median survival was increased to >53 days with a statistically significant survival benefit ($P < 0.0001$; Fig. 4). There was no statistically significant dose-response relationship ($P = 0.0596$). Six animals treated with the high dose of PVS-RIPO survived at the end of the experiment and were followed for 173 days after tumor cell inoculation. Of these, one animal harbored residual tumor detected at necropsy.

Efficacy of Intratumoral PVS-RIPO Injection against Intracerebral MCF-7/HER2-18 Human Breast Cancer Xenografts. As with NM xenografted animals, intracerebral tumor was also consistently evident microscopically 3 days after intracerebral challenge with the MCF-7/HER2-18 cell line. Furthermore, intracerebral tumor challenges with 8×10^5 MCF-7/HER2-18 cells consistently resulted in tumor growth in all rats challenged, and all untreated rats died from intracerebral tumors.

To evaluate toxicity associated with virus treatment, intracerebral administration of PVS-RIPO at a dose of 10^7 pfu/10 μl was compared with treatment with PBS alone in groups of eight and five rats, respectively. At this dose, neither weight loss of >10% nor neurological deficits were observed. Histological examination of brain revealed hemorrhage around the injection site in two rats, possibly caused by the virus injection procedure. There was no evidence of edema, demyelination, or arachnoid fibrosis in the brains of PVS-RIPO-treated rats.

The therapeutic efficacy of intracerebral PVS-RIPO against intracerebral tumor of MCF-7/HER2-18 human breast cancer cells was investigated at two different doses. Treatment of intracerebral MCF-7/HER2-18 human breast cancer cells with 10^7 pfu PVS-RIPO/10 μl 3 days after inoculation of 8×10^5 cells increased median survival to 51 days from 23 days in the UV-inactivated PVS-RIPO-treated groups (Fig. 5). These values represent a 122% increase in median survival ($P < 0.0001$; Fig. 5). In a group receiving a higher dose of 10^9 pfu PVS-RIPO/20 μl, the median survival was increased to 58 days (152%), confirming a statistically significant survival benefit ($P < 0.0001$) but no statistically significant dose-response relationship. Four rats that received the high-dose virus treatment and two animals treated with low-dose virus survived at the end of the experiment and were followed for 159 days after tumor cell inoculation. Necropsy revealed remaining tumor in one of the animals that had received the low-dose treatment.

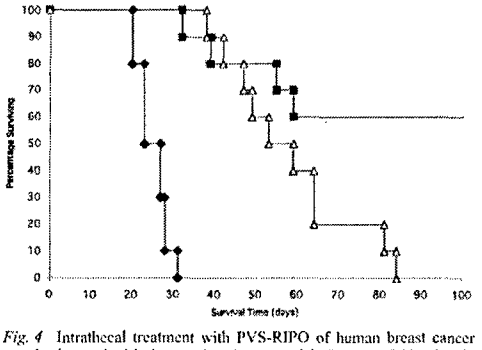

Fig. 4 Intrathecal treatment with PVS-RIPO of human breast cancer neoplastic meningitis in an athymic rat model. Groups of 10 athymic rats harboring intrathecal MCF-7/HER2-18 xenografts (see "Materials and Methods") were treated with PVS-RIPO administered at a dose of 1×10^7 plaque-forming units (pfu)/40 μl (△) or 1×10^9 pfu/40 μl (■), 3 days after tumor cell inoculation. Control animals were treated with UV-inactivated PVS-RIPO (◆; corresponding to 1×10^7 pfu). Survival was plotted over time.

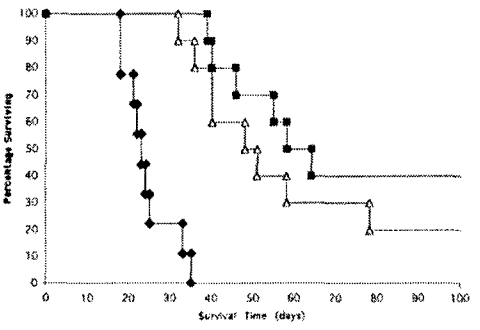

Fig. 5 Regional treatment with PVS-RIPO of breast cancer cerebral metastasis in an athymic rat model. Groups of 10 athymic rats harboring intracerebral MCF-7/HER2-18 xenografts (see "Materials and Methods") were treated with PVS-RIPO administered at a dose of 1×10^7 plaque-forming units (pfu)/10 μl (△) or 1×10^9 pfu/20 μl (■), 3 days after tumor cell inoculation. Control animals were treated with UV-inactivated PVS-RIPO (◆; corresponding to 1×10^7 pfu). Survival was plotted over time.

Stability of the Non-Neuropathogenic Phenotype of PVS-RIPO Replicating in Breast Cancer Cells. To exclude the possibility of PVS-RIPO genetically adapting to neurovirulence on replication in susceptible breast cancer cells, we analyzed virus after 10 serial passages in MCF-7/HER2-18 cells in culture and virus isolated from MCF-7/HER2-18 xenografts of PVS-RIPO-treated rats. Virus recovered after 10 serial passages in MCF-7/HER2-18 cells was subjected to one-step growth curve analysis in MCF-7/HER2-18 and nonpermissive HEK 293 cells (Fig. 6).[4] Furthermore, we performed reverse transcription-PCR sequencing of the genomic region spanning the IRES and the coding region for the capsid proteins for virus recovered after serial passage in culture as well as from PVS-RIPO treated rats (see "Materials and Methods" for details). Neither the virus passaged in cultured MCF-7/HER2-18 cells nor virus associated with intracerebral MCF-7/HER2-18 xenograft tissue in treated rats differed in sequence from the original inoculum. As expected, one-step growth kinetics in

[4] S. A. Moore, M. K. Merrill, and M. Gromeier. Genetic determinants of cell type-specific propagation of poliovirus in HEK 293 cell, submitted for publication.

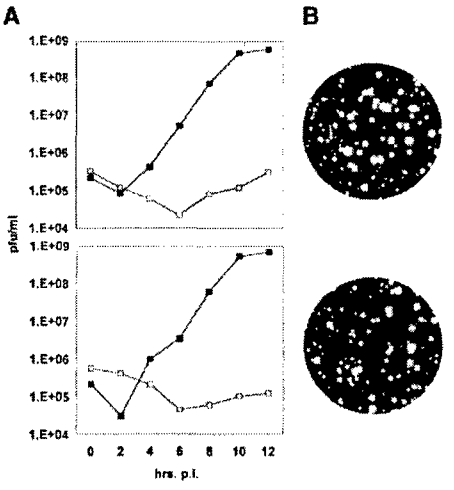

Fig. 6 One-step growth kinetics and plaque phenotype of serially passaged PVS-RIPO. *A*, growth kinetics of PVS-RIPO in MCF-7/HER2-18 breast cancer cells (■) and HEK 293 cells (□) before (*top panel*) and after (*bottom panel*) 10 serial passages in the former. *B*, plaque phenotype of PVS-RIPO before (*top*) and after (*bottom*) serial passaging.

HEK 293 cells of virus obtained after serial passages in MCF-7/HER2-18 cells confirmed the characteristic phenotype of PVS-RIPO (Fig. 6*A*). Accordingly, we did not observe changes in plaque phenotype after serial passaging (Fig. 6*B*). Our findings indicate that the cell type-specific propagation profile of PVS-RIPO does not change on replication in MCF-7/HER2-18 breast cancer cells.

DISCUSSION

Oncolytic agents based on animal viruses, *e.g.*, herpes virus (30), adenovirus (31), reovirus (32), vesicular stomatitis virus (33), and measles virus (34), have been reported to produce remarkable remissions in rodent xenotransplantation tumor models. Although clinical investigation of most of these agents is in initial stages, the outcomes of such trials suggest major obstacles to virus-mediated oncolytic therapy posed by lacking target tropism and tumor cell entry.

Testing against established cancer cell lines, either in culture or as xenografts, remains the mainstay of preclinical evaluation of antineoplastic agents, including oncolytic viruses. Because such cell lines often poorly represent real tumors, antineoplastic effects of oncolytic viruses in clonal cell lines chosen for their favorable response to infection may raise overly optimistic expectations about their behavior in patients. Although mechanisms of virus resistance beyond receptor interaction certainly play a role, the overwhelming importance of viral receptors as susceptibility determinants for viral therapeutics is intuitively obvious. Experimental virus-based therapy, either in the form of gene therapy or oncolytic virus treatment, has generally been administered indiscriminately without prior assaying receptor expression profiles of the tumor target.

We demonstrate here that the PV receptor CD155, a putative immunoglobulin superfamily cell adhesion molecule, is ectopically expressed in breast cancer cells and a significant proportion of breast carcinomas. In contrast, CD155 levels were exceedingly low in organoid cultures of normal human breast epithelium. Physiological CD155 expression occurs in the embryonic ventral neuraxis (35) and may be responsible for PV's predilection for anterior horn motor neurons (35). As with many immunoglobulin superfamily cell adhesion molecules (36), including the rodent CD155 relative Tage4 (37), ectopic CD155 expression has been reported in a number of malignancies including colorectal (38) and neuroectodermal tumors (13). This is supported by evidence for *CD155* regulation by the morphogenic factor *sonic hedgehog* and its downstream effectors of the *gli* family (39). Abnormal activation of *sonic hedgehog* signaling pathways, which are physiologically active during embryogenesis, is a common feature of many carcinomas (40).

Our analyses of the association of CD155 with breast cancer have revealed important limitations of virus-mediated oncolytic therapy. Low expression in several cell lines correlated with resistant subpopulations that survived PVS-RIPO treatment. Accordingly, scant CD155 levels in some tumors indicate that PVS-RIPO may not be a suitable targeting agent for all breast cancers. Evaluation of the relationship of CD155 expression and PV susceptibility in primary explant breast cancer cultures could lend further support to our findings. However, the enormous difficulties in subcultivating primary breast cancer cells and generating culture systems amenable for virological assays (reviewed in Ref. 41) have prevented us from pursuing this. As with other biological therapeutics targeting ectopically expressed cell surface molecules (24), any clinical application of PVS-RIPO against NM or cerebral metastasis secondary to breast cancer would require tumor profiling to determine CD155 expression levels.

Because our expression analyses rely on tissue homogenates, complementary immunohistological assays to elucidate the intratumoral distribution of CD155 would be highly desirable. Immunohistochemical detection of CD155 has been notoriously difficult, and we have been consistently unable to demonstrate CD155 expression patterns unambiguously in human tissues, including the spinal cord anterior horn. This difficulty is likely to result from the exceedingly low levels of CD155, even in high CD155-expressing tumor cell lines exquisitely sensitive to PVS-RIPO [*e.g.*, HeLa cells (42) and MDA-MB-231 cells]. Low CD155 expression levels call for the cumbersome combined antigen capture/Western blot procedure, allowing quantitative detection of CD155 in large samples (>25 μg protein) through prior concentration by antigen capture.

NM and intracerebral metastasis represent lethal final common pathways for a spectrum of malignancies arising in the brain or systemically. The inefficiency of currently available treatment options is a reflection of the unique anatomical structure and physiological conditions prevailing in the CNS (43). Regional delivery, such as injection of therapeutic agents into the interstitium of the tumor or subarachnoid space, bypasses the blood-brain barrier and provides high concentrations of the agent at the tumor site while minimizing systemic exposure (43–46).

Although CD155 expression occurs in primary breast can-

cer tissues, we believe our strategy to be most appropriately directed against metastatic CNS disease. Systemic immunity to PV is universal in vaccinated communities and would be expected to interfere with systemically administered oncolytic agents. However, because immunity to PV extends to the CNS only after PV neuroinvasion, regional intrathecal/intracerebral delivery of oncolytic PV recombinants may provide a unique opportunity to target CD155-expressing cancerous cells with circumvention of preexisting immunity.

Although regional administration of PVS-RIPO improved the survival of NM or intracerebral metastasis xenografted rats, treatment efficacy was not concentration dependent. An incomplete response to virus inoculation could be due to the expansion of virus-resistant populations (as observed in virus-infected monolayer cultures; Fig. 2), possibly relating to low or irregular expression of CD155 in MCF-7/HER2-18 cells (Fig. 1A). Alternatively, more efficient means of intrathecal or interstitial PVS-RIPO delivery, *e.g.*, continuous subarachnoid irrigation with artificial cerebrospinal fluid containing PVS-RIPO or convection-enhanced interstitial administration, may improve intrathecal or intratumoral delivery. We are currently evaluating alternative delivery modes experimentally. Our present studies suggest that intrathecal or intracerebral delivery of PVS-RIPO may be an efficacious and safe treatment of CNS metastasis secondary to breast cancer.

REFERENCES

1. Groves MD. The pathogenesis of neoplastic meningitis. Curr Oncol Rep 2003;5:15–23.

2. Wasserstrom WR, Glass JP, Posner JB. Diagnosis and treatment of leptomeningeal metastases from solid tumors: experience with 90 patients. Cancer (Phila) 1982;49:759–72.

3. Grossman SA, Moynihan TJ. Neoplastic meningitis. Neurol Clin 1991;9:843–56.

4. Ongerboer BW, Somers R, Nooyen WH, et al. Intraventricular methotrexate therapy of leptomeningeal metastasis from breast carcinoma. Neurology 1983;33:1565–72.

5. Theodore WH, Gendelman S. Meningeal carcinomatosis. Arch Neurol 1981;38:696–9.

6. Aparicio A, Chamberlain MC. Neoplastic meningitis. Curr Neurol Neurosci Rep 2002;2:225–35.

7. Berry MP, Jenkin RD, Keen CW, Nair BD, Simpson WJ. Radiation treatment for medulloblastoma: a 21-year review. J Neurosurg 1981;55:43–51.

8. Benz CC, Scott GK, Sarup JC, et al. Estrogen-dependent, tamoxifen-resistant tumorigenic growth of MCF-7 cells transfected with HER2/neu. Breast Cancer Res Treat 1993;24:85–95.

9. Markesbery WR, Brooks WH, Gupta GD, Young AB. Treatment for patients with cerebral metastases. Arch Neurol 1978;35:754–6.

10. Gromeier M. Oncolytic viruses for cancer therapy. Am J Cancer 2003;2:313–23.

11. Gromeier M. Viruses for treating cancer. ASM News 2002;68:438–45.

12. Chiocca EA, Aghi M, Fulci G. Viral therapy for glioblastoma. Cancer J 2003;9:167–79.

13. Gromeier M, Lachmann S, Rosenfeld MR, Gutin PH, Wimmer E. Intergeneric poliovirus recombinants for the treatment of malignant glioma. Proc Natl Acad Sci USA 2000;97:6803–8.

14. Mendelsohn CL, Wimmer E, Racaniello VR. Cellular receptor for poliovirus: molecular cloning, nucleotide sequence, and expression of a new member of the immunoglobulin superfamily. Cell 1989;56:855–65.

15. Koike S, Ise I, Sato Y, et al. A second gene for the African green monkey poliovirus receptor that has no putative N-glycosylation site in the functional N-terminal immunoglobulin-like domain. J Virol 1992;66:7059–66.

16. Ren RB, Constantini F, Gorgacz EJ, Lee JJ, Racaniello VR. Transgenic mice expressing a human poliovirus receptor: a new model for poliomyelitis. Cell 1990;63:353–62.

17. Koike S, Taya C, Kurata T, et al. Transgenic mice susceptible to poliovirus. Proc Natl Acad Sci USA 1991;88:951–5.

18. Jang SK, Krausslich HG, Nicklin MJ, et al. A segment of the 5′ nontranslated region of encephalomyocarditis virus RNA directs internal entry of ribosomes during in vitro translation. J Virol 1988;62:2636–43.

19. Pelletier J, Sonenberg N. Internal initiation of translation of eukaryotic mRNA directed by a sequence derived from poliovirus RNA. Nature (Lond) 1988;334:320–5.

20. Gromeier M, Alexander L, Wimmer E. Internal ribosomal entry site substitution eliminates neurovirulence in intergeneric poliovirus recombinants. Proc Natl Acad Sci USA 1996;93:2370–5.

21. Gromeier M, Bossert B, Arita M, Nomoto A, Wimmer E. Dual stem loops within the poliovirus internal ribosomal entry site control neurovirulence. J Virol 1999;72:958–64.

22. Pestova TV, Kolupaeva VG, Lomakin IB, et al. Molecular mechanisms of translation initiation in eukaryotes. Proc Natl Acad Sci USA 2001;9:7029–36.

23. Dobrikova E, Florez P, Bradrick S, Gromeier M. Activity of a type 1 picornavirus internal ribosomal entry site is determined by sequences within the 3′ non-translated region. Proc Natl Acad Sci USA 2003;100:15125–30.

24. Ross JS, Fletcher JA. The HER-2/neu oncogene in breast cancer: prognostic factor, predictive factor, and target for therapy. Oncologist 1998;3:237–52.

25. Grossi PM, Ochiai H, Archer GE, et al. Efficacy of intracerebral microinfusion of trastuzumab in an athymic rat model of intracerebral metastatic breast cancer. Clin Cancer Res 2003;9:5514–20.

26. Dobrikova E, Florez P, Gromeier M. Structural determinants of insert retention of poliovirus expression vectors with recombinant IRES elements. Virology 2003;311:241–53.

27. Fuchs HE, Archer GE, Colvin OM, et al. Activity of intrathecal 4-hydroperoxycyclophosphamide in a nude rat model of human neoplastic meningitis. Cancer Res 1990;50:1954–9.

28. Kooistra KL, Rodriguez M, Powis G, et al. Development of experimental models for meningeal neoplasia using intrathecal injection of 9L gliosarcoma and Walker 256 carcinoma in the rat. Cancer Res 1986;46:317–23.

29. Kaplan EL, Meier P. Nonparametric estimation from incomplete observations. J Am Stat Assoc 1958;53:457–81.

30. Martuza RL, Malick A, Markert JM, Ruffner KL, Coen DM. Experimental therapy of human glioma by means of a genetically engineered virus mutant. Science (Wash DC) 1991;252:854–6.

31. Bischoff JR, Kirn DH, Williams A, et al. An adenovirus mutant that replicates selectively in p53-deficient human tumor cells. Science (Wash DC) 1996;274:373–6.

32. Coffey MC, Strong JE, Forsyth PA, Lee PW. Reovirus therapy of tumors with activated Ras pathway. Science (Wash DC) 1998;282:1332–4.

33. Stojdl DF, Lichty B, Knowles S, et al. Exploiting tumor-specific defects in the interferon pathway with a previously unknown oncolytic virus. Nat Med 2000;6:821–5.

34. Grote D, Russell SJ, Cornu TI, et al. Live attenuated measles virus induces regression of human lymphoma xenografts in immunodeficient mice. Blood 2001;97:3746–54.

35. Gromeier M, Solecki D, Patel D, Wimmer E. Expression of the human poliovirus receptor/CD155 gene during development of the

CNS: implications for the pathogenesis of poliomyelitis. Virology 2000; 273:259–68.

36. Skubitz AP. Adhesion molecules. Cancer Treat Res 2002;107: 305–29.

37. Chadeneau C, LeCabellec M, LeMoullac B, Meflah K, Denis MG. Over-expression of a novel member of the immunoglobulin superfamily in Min mouse intestinal adenomas. Int J Cancer 1996; 68:817–21.

38. Masson D, Jarry A, Baury B, et al. Overexpression of the CD155 gene in human colorectal carcinoma. Gut 2001;49:236–40.

39. Solecki D, Gromeier M, Bernhardt G, Wimmer E. Expression of the human poliovirus receptor/CD155 gene is activated by sonic hedgehog. J Biol Chem 2002;277:25697–702.

40. Taipale J, Beachy PA. The hedgehog and Wnt signaling pathways in cancer. Nature (Lond) 2001;411:349–54.

41. Band V, Sager R. Distinctive traits of normal and tumor-derived human mammary epithelial cells expressed in a medium that supports long-term growth of both cell types. Proc Natl Acad Sci USA 1989;86: 1249–53.

42. Bernhardt G, Bibb JA, Bradley J, Wimmer E. Molecular characterization of the cellular receptor for poliovirus. Virology 1994;199: 105–13.

43. Zimm S, Wampler GL, Stablein D, Hazra T, Young HF. Intracerebral metastases in solid-tumor patients: natural history and results of treatment. Cancer (Phila) 1981;48:384–94.

44. Sampson JH, Archer GE, Villavicencio AT, et al. Treatment of neoplastic meningitis with intrathecal temozolomide. Clin Cancer Res 1999;5:1183–8.

45. Archer GE, Sampson JH, Lorimer IA, et al. Regional treatment of epidermal growth factor receptor vIII-expressing neoplastic meningitis with a single-chain immunotoxin, MR-1. Clin Cancer Res 1999;5: 2646–52.

46. Bergman I, Barmada MA, Griffin JA, Slamon DJ. Treatment of meningeal breast cancer xenografts in the rat using an anti-P185/Her2 antibody. Clin Cancer Res 2001;7:2050–6.

APPENDIX II
Suggested subject categories: *Proteins/Molecular biology of disease*

Cell-Type Specific Repression of Internal Ribosome Entry Site Activity by the NFAR-1 Complex

Melinda K. Merrill, Elena Y. Dobrikova, and Matthias Gromeier*

Department of Molecular Genetics & Microbiology,

Duke University Medical Center, Durham, NC 27710

*Corresponding Author:
Matthias Gromeier
Dept. of Molecular Genetics & Microbiology
Duke University Medical Center, Box 3020
Durham, NC 27710
PHO: 919-668-6205
FAX: 919-684-8735
Email: grome001@mc.duke.edu

Running title: NFAR-1 proteins repress IRES-driven translation

Character Count: 54988

Abstract

Translation of picornavirus RNA genomes occurs via internal ribosomal entry at elaborately structured 5' untranslated regions. In addition to canonical translation factors this process is likely influenced by *trans*-acting factors determining translation rate. Insertion of a rhinovirus internal ribosomal entry site (IRES) into the poliovirus genome selectively abrogates viral translation and propagation in neurons and, hence, eliminates poliovirus' signature neuropathogenicity. Heterokaryon analyses revealed neuronal *trans*-dominant inhibition to cause this effect, implicating repressive host *trans*-acting factors. We determined that the NFAR-1 complex consisting of double-stranded RNA-binding protein 76 (DRBP76), RNA helicase A and nuclear factor 45 bind the rhinovirus IRES. NFAR-1 proteins associate with the IRES in neuronal, but not in malignant glioma cells. Ribosomal profile analyses suggest that the NFAR-1 complex preferentially associates with the translation apparatus in neuronal cells and arrests translation at the HRV2 IRES. DRBP76 depletion in neuronal cells prevents IRES binding of NFAR-1 proteins and enhances rhinovirus IRES-driven translation and virus propagation. Our observations suggest that DRBP76, and possibly the NFAR-1 complex repress rhinovirus IRES-driven translation in a cell type-specific manner.

Keywords: IRES/NFAR-1/poliovirus/rhinovirus/translation

Introduction

Post-transcriptional regulation constitutes an important level of gene expression control. The global rate of protein synthesis is adjusted in response to changes in the intracellular milieu, generally by modification of translation initiation factors. In addition, translation of many mRNAs is independently regulated by processes targeting their 5' and/or 3' untranslated regions (UTRs). In many cases, specific UTRs serve as anchors for ribonucleoprotein complexes that may alter the conditions for translation of individual messages.

Most known incidences of regulated translation result in repression by interference with initiation events (Gebauer and Hentze, 2004). Unimpeded initiation occurs upon assembly of the eukaryotic initiation factor (eIF) 4F at the cap, recruitment of the 43S pre-initiation complex, scanning, formation of the 48S initiation complex at the initiation codon and 60S ribosomal subunit joining. Translation initiation repressors binding to 5' and 3'UTR structures have been reported to interfere with distinct steps of the initiation cascade. These include obstructed eIF4F cap-assembly (Mendez and Richter, 2001), inhibited stable association of the 40S ribosomal subunit (Gray and Hentze, 1994; Gebauer *et al,* 2003), or blocked 60S ribosomal subunit joining (Ostareck *et al,* 2001).

The plus-strand RNA genomes of *Picornaviridae* feature complex UTRs involved in the regulation of viral gene expression and genome replication. Viral gene expression occurs in competition with cellular mRNAs and involves considerable rearrangement of the host translation machinery by the invading pathogen (Belsham and Jackson, 2000). Accordingly, picornavirus genomes have adopted unconventional features enabling efficient gene expression in a hostile environment. They are uncapped (Nomoto *et al,* 1976) and their uncommonly large and highly structured 5'UTRs contain IRESs that mediate translation initiation in a 5' end, cap-independent manner (Jang *et al,* 1988; Pelletier and Sonenberg, 1988).

Uncommon 5'UTR features and a reliance on IRES-mediated initiation indicate that the requirements for proper initiation at picornavirus genomes differ from those of conventional mRNAs. Indeed, IRES translation is unimpeded by virus-induced cleavage of canonical initiation factors eIF4G and poly(A) binding protein (Etchison *et al,* 1982; Joachims *et al,* 1999), indicating that their involvement in initiation at the IRES deviates from capped mRNAs. Moreover, divergent means of translation initiation may imply the involvement of non-canonical translation factors, i.e. IRES *trans* acting factors (ITAFs) (Belsham and Sonenberg, 1996). Such factors, by virtue of their cell and organ-specific distribution, may determine viral gene

expression, propagation and pathogenesis. For example, neuropathogenicity of the picornavirus Theiler's murine encephalomyelitis virus was reported to be influenced by cell type-specific distribution of an ITAF in mouse brain (Pilipenko *et al,* 2000).

We have reported a striking cell type-specific deficit of translation at the human rhinovirus type 2 (HRV2) IRES in cells of neuronal lineage. This deficit was evident when the HRV2 IRES was inserted into the poliovirus (PV) genome, generating the chimera PV-RIPO (Gromeier *et al,* 1996). The HRV2 IRES in PV-RIPO precludes virus propagation in spinal cord motor neurons and prevents poliomyelitis in mice transgenic for the *human poliovirus receptor/CD155* gene (Gromeier *et al,* 1996) and primates (Gromeier *et al,* 1999).

Cell type-specific incompetence of the HRV2 IRES depresses viral gene expression and propagation in neuron-like cells, but has no effect on viral growth in non-neuronal populations, e.g. malignant glioma (Gromeier *et al,* 2000). This non-permissive phenotype maps to HRV2 IRES stem-loop domains V and VI [sldV/VI; Fig. 1A (Gromeier *et al,* 1999; Campbell *et al,* 2005)] and is co-determined by viral 3'UTR sequences (Dobrikova *et al,* 2003). The observed phenotype suggests involvement of ITAFs regulating viral growth in a cell type-specific manner. Based on *in vitro* studies, a number of HRV ITAFs have been proposed. These include the polypyrimidine tract binding protein (Hunt and Jackson, 1999), upstream of N-ras (Hunt *et al,* 1999) and poly r(C) binding protein 2 (Walter *et al,* 1999).

Here we report HRV2 IRES repression in neuroblast:glioma heterokaryons, implicating neuronal *trans* dominant inhibitors in the cell-type specific growth phenotype of PV-RIPO. We identified five proteins binding to the HRV2 IRES sldV/VI from a neuron-derived cell line by RNA affinity chromatography: the double stranded RNA binding protein 76 (DRBP76), RNA helicase A (RHA), nuclear factor 45 (NF45), insulin-like growth factor II mRNA binding protein-1 (IMP-1) and heterogeneous RNP Q1 (hnRNP Q1). Our analyses focus on DRBP76, RHA, and NF45, which join to form the NFAR-1 protein complex (Liao *et al,* 1998; Reichman *et al,* 2003). Recently, NFAR-1 has been independently reported to bind to flavivirus IRESes (Isken *et al,* 2003). We provide evidence that neuron-specific IRES incompetence results from translation repression by NFAR-1 proteins. We found that IRES binding to NFAR-1 proteins is neuron-specific and depends on DRBP76. Further, translation arrest at the HRV2 IRES coincides with the association of NFAR-1 proteins with the translation apparatus in neuronal cells. DRBP76 knock-down by RNA interference (RNAi) in neuron-like cells induces HRV2 IRES-mediated translation as well as PV-RIPO gene expression and viral growth suggesting that the NFAR-1 complex inhibits PV-RIPO propagation at the level of translation.

Results

Neuron-specific repression of PV-RIPO propagation

Despite unimpeded function in cancer cells, e.g. HeLa, breast cancer or malignant glioma, the HRV2 IRES is severely deficient in neuron-like cells (Gromeier *et al,* 2000; Ochiai *et al,* 2004). This suggests that either cancer-specific inducers or neuronal inhibitors modulate HRV2 IRES activity in a cell type-specific manner. We performed heterokaryon analysis to distinguish cancer- from neuron-specific causes for PV-RIPO's selective growth phenotype. To this end, HRV2 IRES non-permissive neuronal HEK-293 cells (Shaw *et al,* 2002; Campbell *et al,* 2005) and permissive malignant glioma (HTB-14) cells were either fused to themselves or to each other. Fusion was evident by merging of HEK-293 and HTB-14 compartments containing the fluorescent gene products RFP and GFP, respectively: incorporation of HEK-293 mitochondria into HTB-14 cytoplasm was detected 2 hrs post-fusion (Figure 1A). Approximately 80% of co-cultured HEK-293 and HTB-14 cells formed heterokaryons after fusion. Fused HEK-293, HTB-14 or HEK-293/HTB-14 heterokaryons were infected with PV-RIPO 2 hrs post-fusion to monitor viral propagation in one-step growth curves (Figure 1B, C). Fused HTB-14 cells support robust PV-RIPO propagation resembling growth in untreated malignant glioma cells (Gromeier *et al,* 2000). As expected, viral growth was negligible in fused HEK-293 cells reflecting neuronal HRV2 IRES incompetence. Intriguingly, HEK-293/HTB-14 heterokaryons exhibited severely reduced viral propagation with viral titers >100 times below that of fused HTB-14 cells and only slightly elevated over fused HEK-293 cells. Residual growth in treated co-cultures likely occurred in unfused glioma cells or HTB-14 cells fused to each other. These findings indicate that *trans*-dominant inhibitors repress PV-RIPO growth in neuronal cells.

Isolation and identification of HRV2 IRES sldV/VI binding proteins

Since heterokaryon analyses implicated *trans*-acting inhibitors in HRV2 IRES neuronal incompetence, we characterized proteins in neuroblastoma cells binding to the HRV2 IRES. We used IRES sldV/VI for our assays, because genetic experiments mapped neuronal dysfunction to this portion (Gromeier *et al,* 1996; Gromeier *et al,* 1999; Campbell *et al,* 2005).

To identify proteins present in neuroblastoma RSW interacting with HRV2 IRES sldV/VI (Figure 2A), we performed RNA affinity chromatography. RSW was loaded onto a sepharose column coupled to sldV/VI. After extensive washes, bound proteins were eluted with a stepwise KCl-buffer gradient ranging from 300-1000 mM and analyzed by SDS-PAGE and silver stain

(Figure 2B). Six proteins with approximate sizes of 130kD, 97kD, 90kD, 65kD, 63kD, and 45kD were eluted from the column in the 400 mM KCl – 600 mM KCl fractions at levels permitting recovery for sequencing (Figure 2C).

Identification was pursued by mass spectrophotometric analysis of tryptic peptide fragments. The deduced peptide sequences (Table 1) and approximate molecular weights unequivocally identified five proteins: p130 is RHA; p90 is DRBP76; p65 is IMP-1; p63 is hnRNP Q1 and p45 is NF45 (analysis of p97 was inconclusive due to insufficient material). RHA, DRBP76, IMP-1 and hnRNP Q1 contain RNA-binding motifs and have known roles in mRNA stability, localization and translation. DRBP76, RHA and NF45 form the NFAR-1 complex *in vitro* and *in vivo* (Corthesy and Kao, 1994; Kao *et al,* 1994; Liao *et al,* 1998; Parker *et al,* 2001; Isken *et al,* 2003; Reichman *et al,* 2003), and constitute the major component of IRES-binding factors identified in our search.

NFAR-1 subcellular distribution is cell-type specific

A possible involvement of NFAR-1 proteins in the cell type-specific functional deficit of the HRV2 IRES would imply differences in expression, subcellular distribution or availability of this complex in neuronal vs. glioma cells. Therefore, we performed Western blot analyses of nuclear, cytoplasmic and RSW extracts from cells of either origin (Figure 2D). While all NFAR-1 components are present in neuronal and glioma cell lines and are expressed at roughly equivalent levels in the nucleus, they are substantially more abundant in cytoplasmic extracts and RSW in neuronal cells (Figure 2D). Since all steps of the picornaviral life cycle take place in the cytoplasm, the sub-cellular localization of IRES-binding proteins may have profound influence on IRES function.

Binding of NFAR-1 proteins to the HRV2 IRES is neuron-specific

NFAR-1 proteins are expressed in neuronal and glioma cells alike, albeit with distinct intracellular distribution. Therefore, we investigated whether IRES binding of NFAR-1 proteins is cell type-specific by performing comparative affinity chromatography analysis using cytoplasmic extracts from HEK-293 and HTB-14 cells (Figure 3). In accordance with previous observations with RSW (Figure 2B), NFAR-1 proteins in HEK-293 cells efficiently bound to sldV/VI (Figure 3A). Interestingly, however, we did not observe any binding of NFAR-1 components from HTB-14 cells, although they are clearly present in the FT (Figure 3B). This suggests that NFAR-1 proteins exhibit IRES binding in a cell type-specific manner.

To discern independent binding of NFAR-1 components, we investigated IRES affinity in HEK-293 cells depleted of DRBP76 by RNA interference (RNAi). Short hairpin (sh) RNA was employed to knock-down DRBP76 expression using a previously established lentivirus delivery strategy (Figure 3C, D) (Brummelkamp *et al,* 2002; Lee *et al,* 2003). Lentivirus infection and ensuing blasticidin selection did not produce morphological abnormalities or affect the viability of shDRBP76 cells (data not shown), but DRBP76/ILF3 protein levels were dramatically reduced in shDRBP76 cells relative to HEK-293 cells infected with empty retroviral vector (Figure 3D). As expected, DRBP76 association with the IRES diminished in shDRBP76 cells (Figure 3F). However, this was mirrored in decreased RHA binding resulting in unbound RHA in the FT/H200 washes and elution at lower salt concentrations relative to HEK-293 (Figure 3A, F). These findings indicate sldV/VI binding of NFAR-1 proteins to depend on either DRBP76 or the intact NFAR-1 complex.

Since shRNA-mediated depletion was incomplete (compare Figure 3A, F), only partially affected RHA binding and failed to significantly change the association of NF45 with sldV/VI, we added affinity chromatography analyses of immunodepleted HEK-293 extracts. Immunodepletion removed DRBP76 entirely (Figure 3E, G) and abolished association of all NFAR-1 components to IRES sldV/VI (Figure 3G). DRBP76 immunodepletion is likely to also remove its binding partners RHA and NF45 from treated extracts; nevertheless, the absence of any IRES binding of the remainder of these NFAR-1 components in immunodepleted extracts suggests that they are unable to associate with the IRES on their own.

***DRBP76 associates with the HRV2 IRES* in vivo**

DRBP76 specifically interacts with the HRV2 IRES in neuronal, but not malignant glioma cell extracts (Figure 3). Next, we analyzed HRV2 IRES association with DRBP76 *in vivo* through RT-PCR analyses of RNA co-immunoprecipitated with DRBP76 in HEK-293 cells (Figure 4). To demonstrate specific binding of DRBP76, we compared *in vivo* affinity for the HRV2 and PV IRESes. Side-by-side analysis of non-propagating PV-RIPO with PV generating vast amounts of viral RNA in infected HEK-293 cells (Campbell *et al*, 2005) would introduce bias. Therefore, we transfected non-replicating subgenomic RNAs differing only with regard to IRES origin (Figure 4A, B). RT-PCR amplified a cDNA fragment only from RNA co-immunoprecipitating with DRBP in cells containing the HRV2 IRES (Figure 4A); no RT-PCR product was obtained from material immunoprecipitating with DRBP76 in cells transfected with PV subgenomic RNA

(Figure 4B), in the absence of RT enzyme or after immunoprecipitation with non-specific IgG. This demonstrates that DRBP76 specifically associates with the HRV2 IRES *in vivo*.

To examine this interaction in the context of the intact viral genome, we performed DRBP76 immunoprecipitation from PV-RIPO infected HEK-293 cells (Figure 4C-F). As with subgenomic RNA, PV-RIPO cDNA was amplified from DRBP76 immunoprecipitate (Figure 4C). In a positive control, IRES cDNA was amplified from RNA co-immunoprecipitated with the nonstructural PV protein 2C (Figure 4C), which associates with viral RNA in infected cells (Bienz *et al,* 1990). In contrast, the endogenous IRES-containing c-*myc* mRNA did not co-immunoprecipitate with DRBP76, while c-*myc* cDNA was readily amplified from total cellular RNA (Figure 4D).

Reflecting affinity of RHA for DRBP76 (Reichman *et al,* 2003), DRBP76 immunoprecipitation recovered both the antigen and RHA (Figure 4E, F). We conclude that DRBP76, possibly in a complex with RHA, associates with PV-RIPO genomic RNA in infected HEK-293 cells. To verify involvement of RHA and NF45 in this interaction, we attempted to immunoprecipitate viral RNA with α-RHA (a gift from J. Hurwitz) and α-NF45 antibodies (a gift from S.E. Behrens), but RNase contamination prohibited their use in our assay.

The NFAR-1 complex associates with the translation apparatus in HEK-293 cells

Cell type-specific subcellular distribution and IRES binding of NFAR-1 proteins in neuronal cells led us to investigate their association with the translation apparatus. To that end, we performed velocity sedimentation analyses of NFAR-1 proteins in ribosomal profiles *in vivo*. Cytoplasmic extracts of mock or PV-RIPO-infected cells were subjected to density gradient centrifugation/fractionation with concomitant analysis of optical density (Figure 5). Protein composition was assayed in every other fraction while ribosomal and viral RNA (in infected cells) were analyzed in each sample. In uninfected HEK-293 cells, DRBP76 and NF45 co-sediment with free protein, 40S and 60S subunits, mono- and polysomes, while RHA associates exclusively with mono- and polysomes (Figure 5A). We excluded non-specific co-sedimentation of NFAR-1 proteins in macromolecular complexes with polysomal fractions by treating samples with EDTA. Polysome disruption by EDTA releases polysome-associated mRNPs; indeed, EDTA treatment disengaged the NFAR-1 complex to the top of the gradient (Figure 5C). Ribosomal protein S6 (RpS6) marks the presence of ribosomes and tubulin represents free protein.

In PV-RIPO infected HEK-293 cells (Figure 5B) viral RNA is detected mainly in 40S subunit-containing fractions with lesser signal with mono- and disome peaks (Figure 5B). Retention of PV-RIPO RNA with 40S subunits indicates hindrance of translation initiation at the HRV2 IRES prior to subunit joining. PV-RIPO infection of HEK-293 cells dramatically shifts the sedimentation pattern of NFAR-1 proteins: polysomal association was lost by 4 hpi, at which point they are detected almost entirely in fractions containing free protein or both 40S subunits and PV-RIPO RNA (Figure 5B). This effect is not due to a shift of ribosomes from the polysome to the monosome pool because the relative absorbance pattern did not change significantly upon infection (Figure 5A, B). This indicates that polysome abundance and the average number of ribosomes per message are not affected by PV-RIPO infection of HEK-293 cells at 4 hpi. Rather, the shift from polysomal to pre-monosomal fractions may result from virus-induced modification of the NFAR-1 complex in HEK-293 cells.

The NFAR-1 complex does not co-sediment with PV RNA

In contrast to PV-RIPO, wild-type PV's neuropathogenic properties are reflected in robust propagation in cells of neuronal lineage, i.e. HEK-293 (Campbell *et al,* 2005). We analyzed viral RNA and the NFAR-1 complex in ribosomal profiles from PV-infected HEK-293 cells. PV RNA was enriched in polysomal fractions (Figure 5D). As with PV-RIPO-infected HEK-293 cells, NFAR-1 proteins were released to pre-polysomal fractions; however, in contrast to PV-RIPO, their distribution in the gradient did not overlap with viral RNA (Figure 5D).

NFAR-1 protein association with the translation apparatus is reduced in glioma cells

NFAR-1 protein abundance was significantly less in ribosome-containing fractions of HTB-14 glioma relative to HEK-293 cells (Figure 5A, E), consistent with NFAR-1 protein levels in their RSWs (Figure 2D). NF45 and RHA are detected in pre-monosomal and monosomal fractions, while DRBP76 does not associate with ribosomes at all. All NFAR-1 proteins from HTB-14 cell lysates co-sediment with free protein. Our data suggest that NFAR-1 proteins associate with the translation apparatus in HEK-293 cells to a greater extent than in HTB-14 cells

In accordance with efficient viral gene expression and propagation in glioma cells, the bulk of PV-RIPO RNA associates with polysomes in infected HTB-14 cells (Figure 5F). Unlike HEK-293 cells, virus infection barely affects NFAR-1 distribution in the ribosomal profile of HTB-14 cells. Significantly, there is complete separation of NFAR-1 proteins in pre-monosomal and monosomal fractions from translating viral RNA in polysomes.

DRBP76 determines association of PV-RIPO with the translation apparatus

We observed neuron-specific binding of NFAR-1 proteins to the HRV2 IRES (Figure 3) and neuron-specific association with the translation apparatus (Figure 5A). To investigate if ribosomal association of viral RNA in neuronal cells correlates with the distribution of NFAR-1 proteins, we conducted ribosomal profile analyses in DRBP76 depleted HEK-293 cells (Figure 5G, H). DRBP76 depletion interrupts HRV2 IRES binding of all NFAR-1 components (Figure 3F, G) and, thus, may reveal the influence of NFAR-1 proteins on the distribution of viral RNA in the ribosomal profile.

DRBP76 knock-down drastically reduced ribosomal associated DRBP76 and displaced RHA and NF45 from polysomal fractions (Figure 5G). This suggests that polysome association of these proteins in HEK-293 cells hinges at least in part on DRBP76. As a result, NFAR-1 sedimentation patterns in shDRBP76 cells resembled those in HTB-14 cells (Figure 5E, G). DRBP76 depletion in infected HEK-293 cells conversely affected the distribution of PV-RIPO RNA in the ribosomal profile. Displacement of NFAR-1 proteins from polysomal fractions by DRBP76 depletion produced a shift of viral RNA towards mono- and polysomal fractions (Figure 5H). Although the degree of polysome association did not reach that in infected HTB-14 cells, the block of translation processing in HEK-293 cells was relieved (Figure 5B, H). This indicates that inclusion of HRV2 IRES-containing viral genomes in polysomes is induced upon DRBP76 depletion and resulting dissociation of NFAR-1 proteins from polysomes.

DRBP76 knock-down induces PV-RIPO propagation

Our analyses of the NFAR-1 proteins' dynamic association with the translation machinery suggest a role in repression of PV-RIPO propagation in HEK-293 cells. shDRBP76 and control cells, which had been infected with the backbone lentiviral vector and selected for blasticidin resistance, were subjected to synchronized infection with PV-RIPO to establish the kinetics of viral propagation and HRV2-IRES-driven gene expression (Figure 6). DRBP76 depletion substantially elevated viral growth; the maximum progeny yield at 7 hpi in shDRBP76 cells exceeded the controls by approximately 20-fold (Figure 6A). Furthermore, there was a marked increase in viral gene expression (Figure 6B). In contrast, DRBP76 depletion had no effect on virus replication or gene expression of wild-type PV (Figure 6C, D). To exclude non-specific or off-target effects of shRNA-mediated knock-down, we reconstituted the protein in shDRBP76 cells by transfecting a DRBP76 cDNA modified by silent mutagenesis in the region targeted by the shRNA. DRBP76 complementation yielded wild-type levels of the protein (Figure 3D) and

completely reversed the viral growth-enhancing effect of the knock-down (Figure 6A). Similarly, PV-RIPO gene expression was severely depressed upon reconstitution of DRBP76 (Figure 6B).

DRBP76 knock-down induces HRV2 IRES activity

Gene expression and synthesis of minus-strand intermediates at plus-strand RNA virus genomes are intertwined processes involving the same template. Hence, ITAFs conceivably can influence virus propagation at multiple levels. Ribosomal profile analyses of PV-RIPO RNA in HEK-293 cells revealed a block of ribosomal subunit joining and polysome formation at the viral genome in infected cells (Figure 5B). Thus, our observations implicate an inability to properly initiate translation at the HRV2 IRES resulting in inefficient viral gene expression in the defective neuronal propagation of PV-RIPO.

To assess a role for DRBP76 in translation control at the HRV2 IRES, we analyzed the effect of DRBP76 knock-down on translation of HRV2 IRES-driven *renilla luciferase* (*rLuc*) reporters. To separately evaluate an influence of DRBP76 on PV gene expression we constructed analogous PV-IRES containing reporters. The expression constructs contain the known determinants of picornavirus type 1 IRES-driven translation, including the 3'UTR, poly(A) tail, cloverleaf and a portion of the N-terminal viral open reading frame (Dobrikova *et al*, unpublished data) (Figure 6E). shDRBP76 and control cells were co-transfected with IRES reporter RNA and an m^7GTP-capped *firefly luc* (*fLuc*) RNA translating under control of the β-globin 5'UTR (Figure 6E). *Luc* activity was monitored 6 hrs post-transfection in a dual *r/fLuc* reporter assay. While DRBP76 knock-down neither affected cap-dependent reporter translation (data not shown) nor PV IRES-mediated reporter expression, HRV2 IRES-driven translation was induced 3.5-fold (Figure 6F). These observations reflect the shift of PV-RIPO RNA towards polysomal fractions in ribosomal profiles (Figure 5B, H) and elevated PV-RIPO gene expression and replication (Figure 6A, B) in shDRBP76 vis-à-vis HEK-293 cells. Our findings suggest DRBP76 to repress HRV2 IRES-mediated translation initiation, viral gene expression and particle propagation in neurons, probably in concert with its partners of the NFAR-1 complex. DRBP76 depletion did not alter reporter RNA stability in HEK-293 cells (Figure 6G, H), suggesting that the effects on reporter gene expression do not relate to effects on transcript integrity.

Discussion

Insertion of the HRV2 IRES into the PV genome abrogates viral gene expression and propagation in motor neurons (Gromeier *et al*, 1996) but does not affect growth in malignant glioma (Gromeier *et al*, 2000). Neuroblast:glioma heterokaryon analysis revealed *trans*-dominant inhibition of PV-RIPO propagation in neuronal cells. We determined that proteins of the NFAR-1 complex associate with the HRV2 IRES *in vitro* and in virus-infected cells. Association with the IRES specifically occurred with extracts of neuronal-, but not glioma-derived cells. The NFAR-1 proteins preferentially associate with the translation apparatus in neuronal cells; after PV-RIPO infection, the viral RNA is detected in a translation inactive state prior to 60S subunit joining, in a distribution overlapping that of NFAR-1 components. In contrast, PV RNA is efficiently incorporated into polysomes in a distribution distinct from NFAR-1 proteins. Depletion of DRBP76 in neuronal cells diminished IRES-association of the NFAR-1 proteins indicating that IRES binding relies on DRBP76 or, alternatively, requires the intact NFAR-1 complex. DRBP76 depletion coincided with a shift of PV-RIPO RNA towards polysomal association in infected neuronal cells, elevated translation at the HRV2 IRES and significantly enhanced PV-RIPO growth. Taken together, our data suggest that DRBP76 or the intact NFAR-1 complex repress HRV2 IRES-mediated translation in neuronal cells.

DRBP76 contains two dsRNA binding motifs and is almost identical to M phase phosphoprotein 4 (MPP4), nuclear factor 90 (NF90), translation control protein 80 (TCP80) and nuclear factor associated with dsRNA-1 (NFAR-1). It has been assigned several disparate functions (Parker *et al*, 2001), but its effects on translation stand out. DRBP76 binds to acid β-glucosidase mRNA and inhibits translation (Xu and Grabowski, 1999; Xu *et al*, 2000). Moreover, it is a regulator and substrate of the dsRNA-dependent protein kinase PKR, whose capacity to inhibit translation initiation is a key component of the innate antiviral response (Langland *et al*, 1999; Patel *et al*, 1999; Parker *et al*, 2001).

Previous investigations of translation initiation at IRESs have exclusively focused on the identification of cellular RNA-binding proteins that enable IRES function (Pestova *et al*, 2001). However, like the overwhelming majority of translation modulators acting through binding to capped mRNA UTRs (Gebauer and Hentze, 2004), ITAFs may repress IRES activity. Similar to most UTR-binding translation repressors, NFAR-1 proteins appear to disturb translation initiation events. The locus of NFAR-1 binding in the HRV2 IRES (sldV/VI) overlaps with the portal of ribosomal entry on viral RNAs (Hellen *et al*, 1994). The bulk of PV-RIPO RNA is

retained with pre-monosomal fractions, suggesting that NFAR-1 proteins hinder IRES-mediated translation in neuronal cells at a step prior to 60S ribosomal subunit joining.

Interaction of NFAR-1 proteins with the IRES, their association with the translation apparatus and the effect on HRV2 IRES function and PV-RIPO propagation are cell type-specific. In malignant glioma cells permissive for PV-RIPO, NFAR-1 proteins neither bind to the HRV2 IRES nor associate with the translation apparatus, preventing interference with translating viral RNA. Interestingly, RNAi depletion of DRBP76 alone in HEK-293 cells is sufficient to prevent IRES binding and polysome association of NFAR-1 proteins, producing PV-RIPO susceptibility akin to HTB-14 glioma cells. Our observations link HRV2 IRES function to the availability of DRBP76 (or the intact NFAR-1 complex) and the level of its interaction with the translation apparatus. The mechanisms regulating the RNA-binding capacity and ribosome association of DRBP76 have not been characterized, but post-translational modifications and the extent of engagement in RNPs may control the potential for interaction with viral RNA in a cell type-specific manner (Smith *et al,* 2004; Parrott *et al,* 2005; Xu and Grabowski, 2005). Thus, the intracellular microenvironment may balance the availability of RNA-binding proteins for interaction with target messages and their association with the translation machinery. This balance may vary in a cell type-specific manner, resulting in organ-specific IRES performance, which may be difficult to mimic in crude *in vitro* translation extracts.

The natural neuropathogenic properties of PV can be abolished by replacement of its cognate IRES with that of HRV2, incompetent to function in neuronal cells. Wild-type PV readily propagates in neuronal cells, reflecting its neuropathogenic properties, and DRBP76 depletion has no effect on viral propagation or gene expression via its cognate IRES. PV RNA readily integrates into polysomes in infected HEK-293 cells, despite the presence of NFAR-1 proteins in this compartment. Our data illustrate how organ-specific and intracellular distribution of translation factors can determine gene expression, particle propagation and, hence, pathogenic features of viruses. HRVs do not naturally infect the human CNS. However, the major group HRVs have the capacity to target motor neurons via their cellular receptor intercellular adhesion molecule 1 (Dufresne and Gromeier, 2004). The absence of neuropathogenicity with these viruses may be due to repression of viral gene expression by incompatible RNA-protein interactions at the HRV IRES. Cell type-specific restrictions of IRES function mediated by RNA-binding proteins with tissue-specific activity have been exploited for the genetic engineering of attenuated strains (Gromeier *et al,* 1996) or therapeutic targeting of virus propagation to certain cell populations (Gromeier *et al,* 2000).

Materials and Methods

cDNA cloning and in vitro *transcription*

Vectors for *in vitro* synthesis of IRES RNAs were constructed as follows: the HRV2 IRES fragment encompassing the T7 promoter and sldV/VI (nt 434-613) was PCR-amplified with primers (1) 5'-ccggatcctataatacgactcactatagggatgatcctccggcccctgaatgtgg-3' and (2) 5'-ccgaattctgt gcacccatggtgcc-3'. The fragment was digested with *Bam*HI and *Eco*RI for insertion into pBluescriptII SK(+). IRES *rLuc*, and capped *fLuc* reporter constructs were generated as previously described (Campbell *et al,* 2005). Subgenomic viral RNAs were generated by T7-mediated *in vitro* transcription from PV-RIPO or PV cDNA digested with *Sfu*I.

pDRBP76-flag (Patel *et al,* 1999) (a gift from G. Sen, Cleveland Clinic) was used to derive pDRBP76(pTyb2), a rDRBP76 expression vector with a C-terminal intein tag. A PCR product corresponding to the DRBP76 ORF was amplified from pDRBP76-flag using primers (3) 5'-ggattccatatgcgtccaatgcgaatttttgt-3' and (4) 5'-tccccgggtgaagaccaaaatcatgat-3', digested with *Nde*I and *Sma*I and ligated into pTyb2 (NEB). pshDRBP76, encoding a retroviral vector expressing shRNA complementary to DRBP76 mRNA, was generated by annealing (5) 5'-phos-gatgtggatggacaggagttccaaggtgttcaagagtaccttggaacttctgtccatccacttttg-3' and (6) 5'-phos-agctcaaa aagtggatggacagaagttccaaggtatctcttgaacaccttggaactcctgtccatccacggg-3' followed by ligation with pSUPER (Brummelkamp *et al,* 2002) digested with *Eco*RI and *Hin*DIII. The ligation product was digested with *Xba*I *and Cla*I and ligated with pNL-SIN to generate shRNA expressing lentiviruses (Lee *et al,* 2003) (all materials used to generate retroviral vectors were kindly provided by B. Cullen, Duke University). pDRBP76^{mut}, bearing silent mutations in the region targeted by shDRBP76 RNA, was generated by PCR amplification of contiguous fragments with primers (7) 5'-ccaggatccatgcgtccaatgcgaatttt-3' and (8) 5'-ggtttgttcgaaccagcacctcggaatttctggcc-3', and (9) 5'-ggtgctggttcgaacaagaaggtggcg-3' and (10) 5'-gcgaattcgatgaacagcagcagtagg-3'. The resulting PCR products were digested with *Bam*HI and *Sfu*I, or *Sfu*I and *Eco*RI, respectively, and ligated with pcDNA3.1+ (Invitrogen). For RT-PCR amplification of c-*myc* RNA we used primers (11) 5'-gcggatcctaatacgactcactatagggaggacccccgagctgtg-3'and (12) 5'-gttttccactacccgaaa aaaatcc- 3'.

Heterokaryon analysis

HEK-293 cells transfected with pdsRed-mito (BD Biosciences), HTB-14 cells transfected with pEGFP-N1 (BD Biosciences) or a 50:50 combination of these transfected cell lines were plated

overnight in 35mM dishes. The following day the cells were washed with PBS and fused for 10 min at room temperature (rt) with 50% polyethylene glycol (Sigma Aldrich) according to established procedures (Pontecorvo, 1975). Cells were infected at 2 hrs post fusion with PV-RIPO at an MOI of 10. Cell morphology and fusion were visually monitored using an Olympus IX50 fluorescence microscope with a 40X dry objective. Cells were harvested at specified time points and processed for one-step growth curve analysis.

Cell extract preparation, Western blotting, immunodepletion

Nuclear, S10 and RSW extracts of Sk-N-Mc, HEK-293, HTB-14 and DU54 cells were prepared as described before. Cell extracts (0.5 mg/ml) were purified over 3 ml heparin sepharose columns (CL4B heparin sepharose; Roche) before use in RNA affinity chromatography. Western blots were performed as described before (Dobrikova *et al,* 2003) with primary antibodies including α-DRBP76 (Transduction Laboratories); α-RHA (a gift from J. Hurwitz, Memorial Sloan Kettering Cancer Center); α-NF45 (a gift from S. Behrens, Fox Chase Cancer Center); α-tubulin (Sigma); α-ribosomal protein S6 (Cell Signaling) and α-2C (a gift from E. Wimmer, Stony Brook University) .

Immunodepletion was performed as described previously (Waggoner and Sarnow, 1998) with the following modifications: 500 µl protein G (Amersham Pharmacia) was coupled to 3 mg α-DRBP76 antibody and incubated with 2 mg HEK-293 S10 extract for 30 min on ice. The protein G beads were removed by centrifugation. This procedure was repeated four times to remove the protein.

RNA affinity chromatography, mass spectrophotometry and peptide identification

RNA affinity chromatography with HRV2 IRES sldV/VI on CNBr-activated sepharose (Pharmacia) was performed essentially as described before (Borman *et al,* 1993). Fractionated column flow-through and eluates were collected, assayed by SDS-PAGE through 4-12% Bis-Tris NuPAGE gels (Invitrogen) and silver stain. The 400-600 mM KCl eluates were subjected to trichloracetic acid (TCA) precipitation, SDS-PAGE and silver stain. Individual bands were excised and sent to the Mass Spectrometry core facility, University of Massachusetts (Worcester) for identification by tryptic digest and sequencing. Approximately 25% of each protein was sequenced (Table 1).

Immunoprecipitation/RT-PCR analysis

HEK-293 cells were either transfected with subgenomic viral RNAs or infected with PV-RIPO at a multiplicity of infection (MOI) of 100. At 2 hrs post transfection or 4 hpi the cells were rinsed, detached by scraping in PBS, and collected by centrifugation. Immunoprecipitation was carried out at 4°C; the cells were lysed in 200 µl RIPA buffer (50 mM Tris-HCl, pH 8.0, 150 mM KCl, 1mM EGTA; 5mM MgCl2, 0.25% NP-40, 0.05% sodium deoxycholate, 100 U/ml RNase OUT) with gentle rocking for 15 min followed by centrifugation for 10 min at 14,000 rpm. For pre-clearing, the supernatant was treated with 100 µl of 50% protein A sepharose beads (Amersham-Pharmacia) in PBS per ml lysate for 10 min followed by pulse centrifugation. The supernatant was diluted to 1 mg/ml in PBS and incubated overnight with α-DRBP76 antibody at 5 µg/ml. 100 µl of 50% protein A sepharose beads in PBS were added followed by incubation for 1 hr with gentle rocking. The beads were collected by pulse centrifugation followed by 2 washes with ice-cold detergent-free RIPA buffer, and 2 washes with ice-cold water. Total RNA was extracted from the beads using Trizol-LS reagent (Invitrogen) according to the manufacturer's protocol. RNA was analyzed by RT-PCR analysis as described before (Gromeier *et al,* 2000).

Cell culture, virus infections, luc reporter assays

Cell culture and propagation, virus infections and growth assays were performed as described (Gromeier *et al,* 1996; Gromeier *et al,* 2000). DNA and RNA transfections were performed with Lipofectamine 2000 and DMRIE-C reagent, respectively (Invitrogen). DNA was incubated with lipofectamine complexes in OPTI-MEM (Invitrogen) for 20 min and then added to 90% confluent cells in a 10 cm dish containing 15 ml of growth media with 10% FBS. Transfection of reporter RNAs, *luciferase* assays and RNA stability evaluations were performed as described previously (Dobrikova *et al,* 2003).

Density gradient centrifugation, ribosomal profiles

Cell lysates were prepared as described before (Lerner *et al,* 2003). Cells were mock-infected or infected with PV-RIPO at an MOI of 10. At 4 hrs pi cycloheximide (CHX; Sigma) was added to the growth media (0.2 mM for 15 min) at 37°C. The cells were collected in 15 ml of permeabilization buffer (110 mM KOAc, 25 mM HEPES, 2.5 mM $Mg(OAc)_2$, 1 mM EGTA, 1 mM DTT, 1 mM PMSF, 0.2 mM CHX, 10 U/ml RNase OUT), centrifuged, resuspended in polysome extraction buffer (400 mM KOAc, 25 mM HEPES, 15 mM $Mg(OAc)_2$, 2% digitonin, 1 mM DTT, 1 mM PMSF, 0.2 mM CHX, 50 U/ml RNase OUT) and incubated on ice for 30 min. After centrifugation for 10 min at 10,000 rpm at 4°C, 800 µl of the supernatant was layered onto

a 10 ml 10-50% sucrose gradient, centrifuged at 35,000 rpm for 3 hrs at 4°C and fractionated while monitoring UV absorbance at 254 nm. Total RNA was isolated from fractions using Trizol-LS reagent and analyzed by agarose gel electrophoresis to detect rRNA. A portion of each sample was used for RT-PCR to detect viral RNA as described (Gromeier *et al,* 2000). Protein was TCA-precipitated, solubilized in SDS PAGE loading buffer and analyzed by Western blot.

Acknowledgments

We thank Hubert Amrein, Haifan Lin and Shelton Bradrick (Duke University) for critical reading of the manuscript. We thank Bryan Cullen, Rachel Lerner and Chris Nicchitta (Duke University) for technical advice. We are grateful to Ganes Sen (Cleveland Clinics) for providing the pDRBP76-flag expression plasmid; Bryan Cullen (Duke University) for pSUPER, pNL-SIN, pTat, pRev and pHIT-G plasmids; Jerard Hurwitz (Memorial Sloan Kettering Cancer Center) for α-RHA antibody, Sven-Erik Behrens (Fox Chase Cancer Center) for α-NF45 antibody; and Eckard Wimmer (Stony Brook University) for α-2C antibody. This work is supported by PHS Grants CA87537 and NS20023 and Concept Award BC033151 from the Congressionally Directed Medical Breast Cancer Research Program. M.G. is a recipient of a Burroughs Wellcome Career Award in the Biomedical Sciences.

References

Belsham G, Jackson RJ (2000) Translation initiation on picornavirus RNA. In *Translational Control of Gene Expression* Sonenberg N, Hershey JWB, Mathews MB (eds) pp 869-900. Plainview, NY: Cold Spring Harbor Laboratory Press.

Belsham GJ, Sonenberg N (1996) RNA-protein interactions in regulation of picornavirus RNA translation. *Microbiol Rev* **60**: 499-511.

Bienz K, Egger D, Troxler M, Pasamontes L (1990) Structural organization of poliovirus RNA replication is mediated by viral proteins of the P2 genomic region. *J Virol* **64**: 1156-1163.

Borman A, Howell MT, Patton JG, Jackson RJ (1993) The involvement of a spliceosome component in internal initiation of human rhinovirus RNA translation. *J Gen Virol* **74**: 1775-1788.

Brummelkamp TR, Bernards R, Agami R (2002) A system for stable expression of short interfering RNAs in mammalian cells. *Science* **296**: 550-553.

Campbell S, Merrill M, Dobrikova E, Gromeier M (2005) Genetic determinants of cell-type specific poliovirus propagation in HEK 293 cells. *J Virol* **79:** 6281-6290.

Corthesy B, Kao, PN 1994. Purification by DNA affinity chromatography of two polypeptides that contact the NF-AT DNA binding site in the interleukin 2 promoter. *J Biol Chem* **269**: 20682-20690.

Dobrikova E, Florez P, Bradrick S, Gromeier M (2003) Activity of a type 1 picornavirus internal ribosomal entry site is determined by sequences within the 3' nontranslated region. *Proc Natl Acad Sci USA* **100**: 15125-15130.

Duchange N, Pidoux J, Camus E, Sauvaget D (2000) Alternative splicing in the human interleukin enhancer binding factor 3 (ILF3) gene. *Gene* **261**: 345-353.

Dufresne AT, Gromeier M (2004) A nonpolio enterovirus with respiratory tropism causes poliomyelitis in intercellular adhesion molecule 1 transgenic mice. *Proc Natl Acad Sci USA* **101**: 13636-13641.

Etchison D, Milburn SC, Edery I, Sonenberg N, Hershey JW (1982) Inhibition of HeLa cell protein synthesis following poliovirus infection correlates with the proteolysis of a 220,000-dalton polypeptide associated with eucaryotic initiation factor 3 and a cap binding protein complex. *J Biol Chem* **257**: 14806-14810.

Gebauer F, Grskovic M, Hentze MW (2003) Drosophila sex-lethal inhibits the stable association of the 40S ribosomal subunit with msl-2 mRNA. *Mol Cell* **11**: 1397-1404.

Gebauer F, Hentze MW (2004) Molecular mechanisms of translational control. *Nat Rev Mol Cell Biol* **5**: 827-835.

Gray NK, Hentze MW (1994) Iron regulatory protein prevents binding of the 43S translation pre-initiation complex to ferritin and eALAS mRNAs. *EMBO J* **13**: 3882-3891.

Gromeier M, Alexander L, Wimmer E (1996) Internal ribosomal entry site substitution eliminates neurovirulence in intergeneric poliovirus recombinants. *Proc Natl Acad Sci USA* **93**: 2370-2375.

Gromeier M, Bossert B, Arita A, Nomoto A, Wimmer, E (1999) Dual stem loops within the poliovirus internal ribosomal entry site control neurovirulence. *J Virol* **73**: 958-964.

Gromeier M, Lachmann S, Rosenfeld MR, Gutin PH, Wimmer, E (2000) Intergeneric poliovirus recombinants for the treatment of malignant glioma. *Proc Natl Acad Sci USA* **97**: 6803-6808.

Hellen CU, Pestova TV, Wimmer E (1994) Effect of mutations downstream of the internal ribosome entry site on initiation of poliovirus protein synthesis. *J Virol* **68**: 6312-6322.

Hunt SL, Hsuan JJ, Totty N, Jackson RJ (1999) Unr, a cellular cytoplasmic RNA-binding protein with five cold-shock domains, is required for internal initiation of translation of human rhinovirus RNA. *Genes Dev* **13**: 437-448.

Hunt SL, Jackson RJ (1999) Polypyrimidine-tract binding protein (PTB) is necessary, but not sufficient, for efficient internal initiation of translation of human rhinovirus-2 RNA. *RNA* **5**: 344-359.

Isken O, Grassmann CW, Sarisky RT, Kann M, Zhang S, Grosse F, Kao PN, Behrens SE (2003) Members of the NF90/NFAR protein group are involved in the life cycle of a positive-strand RNA virus. *EMBO J* **22**: 5655-5665.

Jang SK, Krausslich HG, Nicklin MJ, Duke GM, Palmenberg AC, Wimmer E (1988) A segment of the 5' nontranslated region of encephalomyocarditis virus RNA directs internal entry of ribosomes during in vitro translation. *J Virol* **62**: 2636-2643.

Joachims M, Van Breugel PC, Lloyd RE (1999) Cleavage of poly(A)-binding protein by enterovirus proteases concurrent with inhibition of translation in vitro. *J Virol* **73**: 718-727.

Kao PN, Chen L, Brock G, Ng J, Kenny J, Smith AJ, Corthesy B (1994) Cloning and expression of cyclosporin A- and FK506-sensitive nuclear factor of activated T-cells: NF45 and NF90. *J Biol Chem* **269**: 20691-20699.

Langland JO, Kao PN, Jacobs BL (1999) Nuclear factor-90 of activated T-cells: A double-stranded RNA-binding protein and substrate for the double-stranded RNA-dependent protein kinase, PKR. *Biochemistry* **38**: 6361-6368.

Lee MT, Coburn GA, McClure MO, Cullen BR (2003) Inhibition of human immunodeficiency virus type 1 replication in primary macrophages by using Tat- or CCR5-specific small interfering RNAs expressed from a lentivirus vector. *J Virol* **77**: 11964-11972.

Lerner RS, Seiser RM, Zheng T, Lager PJ, Reedy MC, Keene JD, Nicchitta CV (2003) Partitioning and translation of mRNAs encoding soluble proteins on membrane-bound ribosomes. *RNA* **9**: 1123-1137.

Liao HJ, Kobayashi R, Mathews MB (1998) Activities of adenovirus virus-associated RNAs: purification and characterization of RNA binding proteins. *Proc Natl Acad Sci USA* **95**: 8514-8519.

Mendez R, Richter JD (2001) Translational control by CPEB: a means to the end. *Nat Rev Mol Cell Biol* **2**: 521-529.

Nomoto A, Lee YF, Wimmer E (1976) The 5' end of poliovirus mRNA is not capped with m7G(5')ppp(5')Np. *Proc Natl Acad Sci USA* **73**: 375-380.

Ochiai H, Moore SA, Archer GE, Okamura T, Chewning TA, Marks JR, Sampson JH, Gromeier M (2004) Treatment of intracerebral neoplasia and neoplastic meningitis with regional delivery of oncolytic recombinant poliovirus. *Clin Cancer Res* **10**: 4831-4838.

Ostareck DH, Ostareck-Lederer A, Shatsky IN, Hentze MW (2001) Lipoxygenase mRNA silencing in erythroid differentiation: The 3'UTR regulatory complex controls 60S ribosomal subunit joining. *Cell* **104**: 281-290.

Parker LM, Fierro-Monti I, Reichman TW, Gunnery S, Mathews MB (2001) Double-stranded RNA-binding proteins and the control of protein synthesis and cell growth. *Cold Spring Harb Symp Quant Biol* **66**: 485-497.

Parrott AM, Walsh MR, Reichman TW, Mathews MB (2005) RNA binding and phosphorylation determine the intracellular distribution of nuclear factors 90 and 110. *J Mol Biol* **348**: 281-293.

Patel RC, Vestal DJ, Xu Z, Bandyopadhyay S, Guo W, Erme SM, Williams BR, Sen GC (1999) DRBP76, a double-stranded RNA-binding nuclear protein, is phosphorylated by the interferon-induced protein kinase, PKR. *J Biol Chem* **274**: 20432-20437.

Pelletier J, Sonenberg N (1988) Internal initiation of translation of eukaryotic mRNA directed by a sequence derived from poliovirus RNA. *Nature* **334**: 320-325.

Pestova TV, Kolupaeva VG, Lomakin IB, Pilipenko EV, Shatsky IN, Agol VI, Hellen CU (2001) Molecular mechanisms of translation initiation in eukaryotes. *Proc Natl Acad Sci USA* **98**: 7029-7036.

Pilipenko EV, Pestova TV, Kolupaeva VG, Khitrina EV, Poperechnaya AN, Agol VI, Hellen CU (2000) A cell cycle-dependent protein serves as a template-specific translation initiation factor. *Genes Dev* **14**: 2028-2045.

Pontecorvo G (1975) Production of mammalian somatic cell hybrids by means of polyethylene glycol treatment. *Somatic Cell Genet* **1**: 397-400.

Reichman TW, Parrott AM, Fierro-Monti I, Caron DJ, Kao PN, Lee CG, Li H, Mathews MB (2003) Selective regulation of gene expression by nuclear factor 110, a member of the NF90 family of double-stranded RNA-binding proteins. *J Mol Biol* **332**: 85-98.

Shaw G, Morse S, Ararat M, Graham FL (2002) Preferential transformation of human neuronal cells by human adenoviruses and the origin of HEK 293 cells. *Faseb J* **16**: 869-871.

Smith WA, Schurter BT, Wong-Staal F, David M. 2004. Arginine methylation of RNA helicase a determines its subcellular localization. *J Biol Chem* **279**: 22795-22798.

Waggoner S, Sarnow P (1998) Viral ribonucleoprotein complex formation and nucleolar-cytoplasmic relocalization of nucleolin in poliovirus-infected cells. *J Virol* **72**: 6699-6709.

Walter BL, Nguyen JH, Ehrenfeld E, Semler BL (1999) Differential utilization of poly(rC) binding protein 2 in translation directed by picornavirus IRES elements. *RNA* **5**: 1570-1585.

Xu YH, Busald C, Grabowski GA (2000) Reconstitution of TCP80/NF90 translation inhibition activity in insect cells. *Mol Genet Metab* **70**: 106-115.

Xu YH, Grabowski GA (1999) Molecular cloning and characterization of a translational inhibitory protein that binds to coding sequences of human acid beta-glucosidase and other mRNAs. *Mol Genet Metab* **68**: 441-454.

Xu YH, Grabowski GA (2005) Translation modulation of acid beta-glucosidase in HepG2 cells: participation of the PKC pathway. *Mol Genet Metab* **84**: 252-264.

Figure Legends

Figure 1 HEK-293/HTB-14 heterokaryon analyses. **(A)** Fluorescence microscopy of fused HTB-14 cells, fused HEK-293 cells and HEK-293/HTB-14 heterokaryons 2 hrs post fusion. HTB-14 cells express GFP throughout the cytoplasm and HEK-293 cells express RFP targeted to mitochondria; note overlapping fluorescent compartments in heterokaryons. **(B)** One-step growth curve analysis of PV-RIPO propagation in fused HTB-14 cells (♦), fused HEK-293 cells (■), and HEK-293/HTB-14 heterokaryons (▲). **(C)** Plaque assay of cell lysate diluents from fused HTB-14, HEK-293, and HEK-293/HTB-14 heterokaryons at 0 hrs post infection (hpi) and 6 hpi with PV-RIPO.

Figure 2 HRV2 IRES sldV/VI RNA affinity chromatography. **(A)** Predicted secondary structure of the HRV2 IRES element; numbering refers to the nt positions relative to the 5' end of the genomic RNA. IRES stem loop domains are marked by roman numerals and the sldV/VI fragment used for our studies is boxed. The initiation codon is indicated by an asterisk. **(B)** Neuroblastoma RSW (CE; lane 1) was applied to a sldV/VI RNA affinity column. After collection of flow-through (FT; lane 2), the column was washed with H200 (lanes 3-8) and eluted with a 300-1000 mM KCl gradient (lanes 9-15). Column fractions were resolved by SDS-PAGE and silver stained. **(C)** Eluates corresponding to H400-H600 (lanes 10-12) were concentrated, resolved by SDS-PAGE gel and the protein bands were silver stained and excised for sequencing. **(D)** NFAR-1 expression profile in cultured cell lines. Sk-N-Mc neuroblastoma and HEK-293 neuroblast cell extracts and HTB-14 and DU54 glioma cell extracts (5μg/lane) were resolved by SDS-PAGE and analyzed by Western blot with α-RHA, α-DRBP76, α-NF45 and α-tubulin antibodies as indicated (N=nuclear fraction; S10=crude cytoplasmic fraction; RSW=ribosomal salt wash). The slower migrating protein detected by the α-DRBP76 antibody corresponds to ILF-3, a DRBP76 isoform (Duchange *et al*, 2000).

Figure 3 Comparative RNA affinity chromatography. HEK-293 **(A)**, HTB-14 **(B)**, shDRBP76 **(F)** and DRBP76 immunodepleted HEK-293 **(G)** S10 cytoplasmic lysates were applied to sldV/VI RNA affinity columns. After collection of FT (lane 1), the column was washed with H200 (lanes 2-3) and eluted with a 400-1000 mM KCl gradient (lanes 4-11). Column fractions were analyzed by SDS-PAGE and silver stain or Western blot with α-RHA, α-DRBP76 and α-

NF45 antibodies as indicated. **(C)** Sequence and predicted structure of the DRBP76 shRNA. **(D)** Western blot analysis of control cells (lane 1), shDRBP76 cells (lane 2), and shDRBP76 cells transfected with DRBP76^{mut} DNA (lane 3) using α-DRBP76 and α-tubulin antibodies as indicated. **(E)** Western blot analysis of HEK-293 S10 (lane 1) and DRBP76 immunodepleted HEK-293 S10 lysate (lane 2) using α-DRBP76 and α-tubulin antibodies as shown.

Figure 4 Immunoprecipitation/RT-PCR of DRBP76 from HEK-293 cells transfected with PV-RIPO **(A)** and PV **(B)** subgenomic RNAs, as well as cells infected with PV-RIPO **(C, D)**. Total RNA, or immunoprecipitates generated with α-DRBP76, non-specific IgG or α-2C antibodies as indicated, were subjected to RT-PCR amplification of the HRV2 **(A, C)** or PV **(B)** IRES or the c-*myc* 5'UTR **(D)**. -RT and +RT represent reactions carried out in the absence and presence of reverse transcriptase as indicated. Western blot detection of DRBP76 **(E)** and RHA **(F)** in the immunoprecipitate generated with α-DRBP76 or non-specific IgG antibodies.

Figure 5 Ribosomal sedimentation profiles in HEK-293, HTB-14 and shDRBP76 cells. Top panels; A254 absorption spectra of lysates generated from mock infected HEK-293 **(A)**, HTB-14 **(E)** and shDRBP76 cells **(G)**, or HEK-293 lysates treated with EDTA **(C)**. Bottom panels; A254 absorption spectra of lysates generated from PV-RIPO infected HEK-293 **(B)**, HTB-14 **(F)**, shDRBP76 **(H)** or PV infected HEK-293 **(D)** cells. Lysates from infected cells were generated 4 hpi. Western blot analyses of protein from every other gradient fraction were performed with α-RHA, α-DRBP76, α-NF45, α-RpS6 and α-tubulin antibodies, as indicated. Viral cDNA corresponding to the IRES region was amplified by RT-PCR and rRNA was analyzed from total RNA purified from every fraction in the gradient.

Figure 6. DRBP76 depletion enhances HRV2 IRES-driven reporter translation, PV-RIPO gene expression and virus propagation in HEK-293 cells. One step growth curve analysis of PV-RIPO **(A)** and PV **(C)** propagation in control cells (■), shDRBP76 cells (●) or shDRBP76 cells transfected with pDRBP76^{mut} DNA (◆). Western blot analysis of PV-RIPO **(B)** and PV **(D)** gene expression in infected cell lysates at specified hpi using α-2C antibody. **(E)** Schematic depiction of the HRV2 IRES *rLuc* reporter expression construct (top) and a capped *fLuc* reporter construct containing the β-globin 5'UTR (bottom). **(F)** Effect of DRBP76 knock-down on HRV2 (■) or PV (▩) IRES-driven *rLuc* translation relative to capped *fLuc* translation in

shDRBP76 and control HEK-293 cells. The data are the average of 3 independent assays plus standard error and are expressed as fold induction of *rLuc* activity relative to *fLuc* activity. **(G)** DRBP76 depletion does not affect the stability of the HRV2 IRES reporter construct *in vivo*. [α^{32}P]-labeled HRV2 IRES reporter RNAs recovered from shDRBP76 or control cells were analyzed on a denaturing polyacrylamide gel. **(H)** Kinetics of labeled HRV2 IRES reporter RNA decay by phosphorimager quantification in control (■) and shDRBP76 cells (●).

Table 1 Tryptic peptide fragment sequences.

Peptide	Measured Mass (m/z Da)	Computed Mass (MH^+, Da)	Residues	Peptide Sequence
DRBP76:				
1	707.4100	707.3629	215-219	(K)WFQAR(A)
2	878.4800	878.4327	6-12	(I)FVNDDR(H)
3	984.6500	984.5631	324-332	(R)LAAFGQLHK(V)
4	1020.6100	1020.5730	578-587	(K)AYAALAALEK(L)
5	1056.7000	1056.5763	333-342	(K)VLGMDPLPSK(M)
6	1301.8300	1301.7581	409-419	(R)LNQLKPGLQYK(L)
7	1328.8200	1328.6455	397-408	(K)AEPPQAMNALMR(L)
8	1368.8800	1368.6872	312-323	(R)EDITQSAQHALR(L)
9	1443.9400	1443.7266	461-474	(K)VLQDMGLPTGAEGR(D)
10	1780.9200	1780.9054	309-323	(R)QQREDITQSAQHALR(L)
11	1910.0900	1909.9871	183-200	(K)VLAGETLSVNDPPDVLDR(Q)
12	2671.2100	2671.2422	18-40	(K)HSSVYPTQEELEAVQNMVSHTER(A)
NF45:				
1	886.5100	886.4899	320-327	(R)ILSHGGFR(K)
2	1041.6800	1041.6421	197-206	(K)VLQSALAAIR(H)
3	1236.8700	1236.7680	175-185	(K)ILITTVPPNLR(K)
4	1732.0800	1731.9169	44-59	(R)VKPAPDETSFSEALLK(R)
5	1888.1100	1888.0180	44-60	(R)VKPAPDETSFSEALLKR(N)
6	2099.1600	2099.0984	61-80	(R)NQDLAPNSAEQAILALVTK(I)
7	2582.2800	2582.3830	81-103	(K)INNVIDNLIVAPGTFEVQIEEVR(Q)
RHA:				
1	758.4400	758.4273	25-311	(R)AVGNKNR(Q)
2	758.4400	758.4313	900-905	(R)LGYIHR(N)
3	777.3900	777.4115	1131-1136	(R)MLNMIR(Q)
4	986.5400	986.5060	1155-1163	(R)YGDGPRPPK(M)
5	1003.5900	1003.5940	810-819	(R)LGGIGQFLAK(A)
6	1025.5600	1025.5420	64-71	(R)DFVNYLVR(I)
7	1075.6200	1075.5536	315-323	(K)LAQFEPSQR(Q)
8	1087.6600	1087.6224	447-456	(R)RISAVSVAER(V)
9	1186.6300	1186.5857	142-151	(R)GANLKDYYSR(K)
10	1186.6300	1186.5605	200-209	(K)YTQVGPDHNR(S)
11	1464.8500	1464.8327	681-692	(R)YQILPLHSQIPR(E)
12	1714.9000	1714.9016	1075-1089	(K)VQSDGQIVLVDDWIK(L)
13	1741.8900	1741.8608	838-853	(R)ELDALDANDELTPLGR(I)
14	1872.0000	1872.1033	1058-1074	(K)GMTLVPPLQLLLFASKK(V)*
15	1872.0000	1872.0125	1137-1154	(R)QISRPSAAGINLMIGSTR(Y)
16	1971.0300	1971.0551	820-837	(K)AIEPPPLDAVIEAEHTLR(E)
17	2050.0000	1050.0245	418-434	(K)TTQVPQFILDDFIQNDR(A)
hnRNP Q1:				
1	784.4300	784.3994	357-363	(K)AFSQFGK(L)
2	860.6100	860.5246	245-252	(R)LFVGSIPK(S)
3	860.6100	860.5722	337-343	(K)VKVLFVR(N)
4	927.5800	927.5052	185-192	(K)AGPIWDLR(L)
5	1058.6200	1058.5383	222-229	(K)LYNNHEIR(S)
6	1182.7300	1182.6271	357-366	(K)AFSQFGKLER(V)
7	1260.7500	1260.6444	193-203	(R)LMMDPLTGLNR(G)
8	1276.7600	1276.6394	193-203	(R)LMMDPLTGLNR(G)*
9	1311.7600	1311.6654	131-142	(R)TGYTLDVTTGQR(K)
10	1473.9100	1473.7801	344-356	(R)NLANTVTEEILEK(A)
11	1593.9500	1593.8052	172-184	(R)DLFEDELVPLFEK(A)
IMP-1:				
1	736.4500	736.3854	168-174	(R)RGGFGSR(G)
2	772.4800	772.4681	291-297	(R)LIGKEGR(N)
3	837.5100	837.4947	87-93	(R)NIPPQLR(W)
4	1096.6600	1096.6115	191-199	(K)QQQVDIPLR(L)
5	1140.7300	1140.6278	281-290	(K)ILAHNNFVGR(L)
6	1309.8000	1309.7116	441-452	(K)IAPPETPDSKVR(M)
7	1430.8500	1430.7717	453-465	(R)MVHTGPPEAQFK(A)
8	1521.8300	1521.7636	539-551	(K)HGHFYASQMAQR(K)
9	1853.0500	1852.9961	21-36	(K)VFAEHKISYSGQFLVK(S)
10	1853.0500	1852.8356	331-345	(K)GAIENCCRAEQEIMK(K)*
11	1853.0500	1853.0133	509-525	(K)TVNELQNLTAAEVVVPR(D)
12	1872.9600	1872.9092	151-167	(K)VSYIPDEQIAQGPENGR(R)
13	2029.0500	2029.0103	151-168	(K)VSYIPDEQIAQGPENGRR(G)
14	2131.2100	2131.1624	179-199	(R)QGSPVAAGAPAKQQQVDIPLR(L)

Figure 1

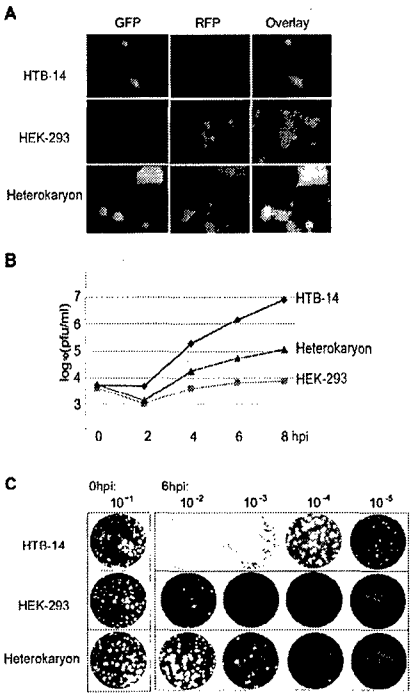

Figure 2

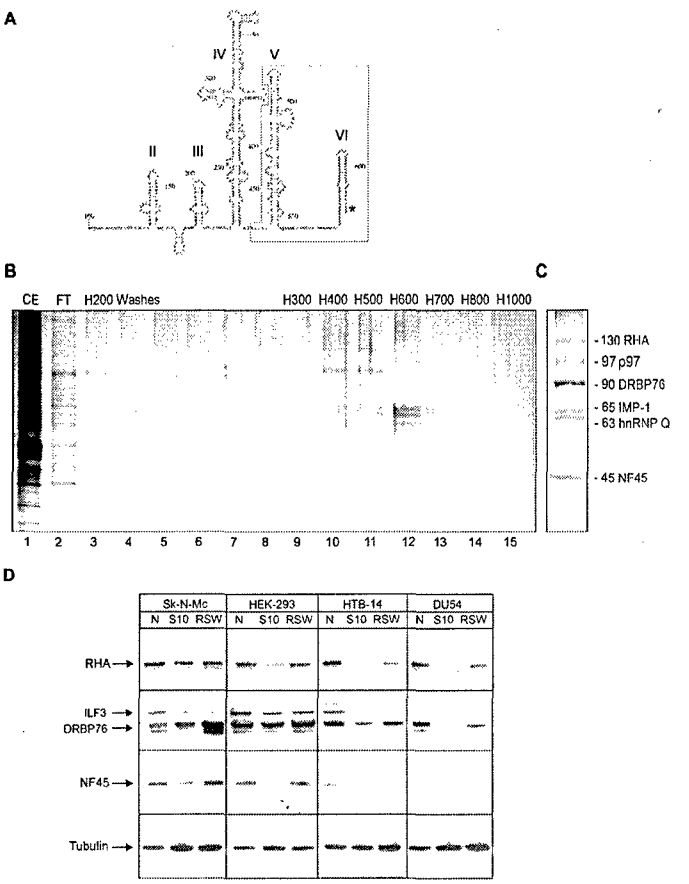

Figure 3

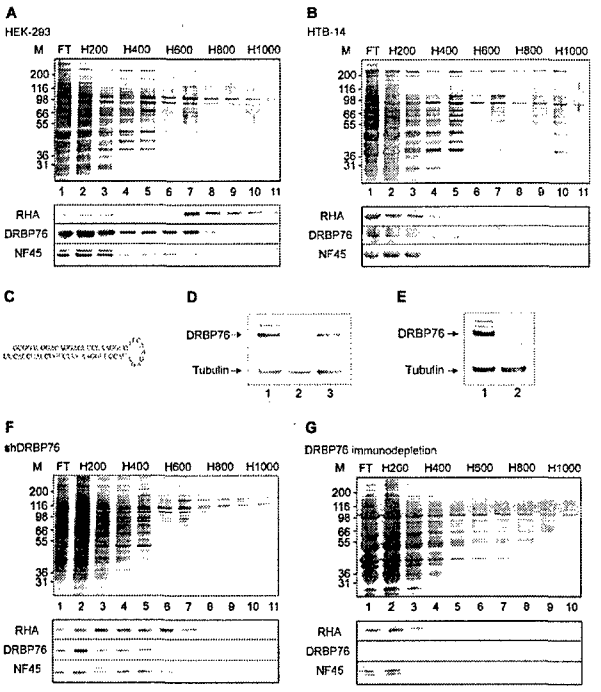

Figure 4